Geotech Geol Eng
https://doi.org/10.1007/s10706-023-02618-y

ORIGINAL PAPER

Structural Response of Large Span Underground Spaces Due to Adjacent Excavation

Dariush Mohammadi · Davoud Parsapour

Received: 22 October 2022 / Accepted: 11 August 2023

Abstract Underground structures such as tunnels, powerhouse caverns and subway stations, as a main structure, have different side structures that are considered for utility and access. Side structures have usually been constructed adjacent to the main structure in the form of gallery and shaft. The study focuses on the influence of construction of a nearby link tunnel between line 6 and 7 of Tehran metro in Iran, as a side structure, on existing F6G7 exchange subway station as a main structure using 3D numerical model, analytical and observational method. When a structural element is deformed, the internal forces are induced within it, therefore the host ground deformation due to adjacent excavation is known as a controlling factor to ensure the structural adequacy of existed underground structure. This goal will not be achieved unless the adjacent structure construction process is selected with proper staged construction and accepted ground deformation. Eight different schemes for excavation of link tunnel adjacent to F6 station were evaluated. The state of stress surrounding non-circular link tunnel, induced internal forces and structural design of F6 station were assessed based on eight construction schemes for link tunnel. The results show that partial excavation, using invert in initial support system, using pre-supporting system in link tunnel staged construction process have significant effect to reduce the host ground deformation and structural responses of F6 subway station consequently.

Keywords Tehran metro · Internal forces · Conformal mapping · Complex variable · Link tunnel

1 Introduction

Cities are the collection of different structures that have been located adjacent and near together, so the surface and subsurface structures may be constructed in the close distance themselves. Meanwhile, the new underground excavations such as urban basements, tunnels and underground spaces may be excavated adjacent of an existed underground structure. The inevitable influence of a new excavation on nearby structures is of great concern in practice, which can negatively effect on serviceability and operation of existed structure (Liang et al. 2016).

Underground excavation causes an alternation in the state of the in-situ stresses of ground (U.S. FHWA, 2009; Valizadeh Kivi et al. 2012), in the other words, when an underground structure is constructed, the ground deformations and stress redistribution processes occur in the zone of influence of underground

D. Mohammadi (✉)
Department of Mining Engineering, Amirkabir University of Technology, Tehran, Iran
e-mail: d.mohammadi@aut.ac.ir

D. Mohammadi · D. Parsapour
Department of Civil and Environmental Engineering, Amirkabir University of Technology, Tehran, Iran

Published online: 13 September 2023

structure until a stable state of equilibrium is reached. The host ground equilibrium of excited underground structure is redistributed by excavating an new adjacent structure, so to reach a stable state of equilibrium, new deformation and internal forces (e.g. bending moment, axial force and shear force) will be induced in the structural elements of existed underground structure (Sagaseta et al. 1980; Franzius 2003; Li and Yuan 2012; Fang et al. 2016).

Underground structures like tunnels, powerhouse caverns and subway stations have side structures that are considered for facilities, access, connection, ventilation and emergency conditions beside the main structure. Side structure construction as a new structure makes adjacent excavation problem to existed structures, so it is important that the existed structure is considered in the design process of new adjacent structure.

Many approaches have been proposed to assess the excavation of new underground structure on existed tunnels, pipe lines and underground structures. These approaches can be divided into the physical model, site observation, empirical method, analytical method and numerical method. Kim et al. (1996) proposed some physical models for parallel and perpendicular tunnels in clay and the in-situ stress redistribution and ground loss were assessed. In Kyoto, Japan, Yamaguchi et al. (1998) compared the behavior of four parallel tunnels that were excavated by TBM. Asano et al. (2003) assessed adjacent tunnels based on observational method. Ng et al. (2004) reported the multiple interaction problem between parallel twin NATM tunnels. Klar et al. (2005, 2007) and Vorster et al. (2005) proposed the elastic continuum solution and the closed-form Winkler model solution to calculate the tunnel and pipelines interaction. Liu et al. (2009) studied the new tunnel construction above the exiting tunnel in Sydney, Australia. Chakeri et al. (2011) conducted the ground stress distribution and deformations using 3D numerical model during the double arch Tohid urban tunnel driving perpendicularly the Tehran metro line 4. Hosseini et al. (2011) examined the intersection area of the line 3 and 7 tunnel of Tehran metro by three-dimensional finite element method. Sadaghiani and Mirhadi (2013) investigated the effect of Tehran metro line 7 tunnel that was excavated by TBM parallelly beneath the double arch Tohid urban tunnel. Zhang and Huang (2014) introduced an analytical solution to calculate the deformation of interaction area of two tunnels. Liang et al. (2016) proposed an analytical method to investigate the effects of above-crossing tunnelling on the existing shield tunnels. Eslami and Golshani (2017) investigated the construction of Q7 underground double-deck subway station in Tehran metro line 7 and its interaction with adjacent structures. Jin et al. (2018) evaluated the twin tunnels of line 9 of Shenzhen metro beneath line 4 existing tunnel. Pan et al. (2018) analyzed the influence of new cross tunnel construction on the existing tunnel in Fuzhou, China, using a three-dimensional finite element model. Mohammadi et al. (2021) assessed the interaction of Earth Pressure Balance Machine (EPBM) during tunneling on sub-surface obstacles like wells and cavities in line 7 Tehran metro, Iran. Huang et al. (2021) optimized the shield tunneling parameters of metro tunnel in under crossing zone of an existing high-speed railway tunnel using field test. Zheng et al. (2021) analyzed the double-line tunnels passing under the station under close distance construction using 3D numerical model. Liu et al. (2021) proposed deformation and structural force of upper tunnel considering the interaction of undercrossing. Zhou et al. (2021) predicted surface settlement by excavating the twin tunnels. Tahmasebi et al. (2022) studied on a case study, Zarbalizadeh NATM Tunnel in Tehran, Iran using three-dimensional probabilistic analysis of the Surface Settlement. Zhou et al. (2022) studied on mechanical response of supporting structure of closely spaced twin tunnels using field monitoring. Ding et al. (2023) proposed a simplified analytical method on the deformation of existing tunnel caused by under-crossing of shield tunneling.

In the current study, a brief overview of intersection area of line 6 and 7 of Tehran Metro is first illustrated and then the statement of problem will be described. The numerical simulation procedure for link tunnel—F6 subway station interaction analysis and the validation procedure by analytical and observational method will be discussed in detail. Then the numerical analysis output for each construction scheme will be employed to compare construction techniques by evaluating their ground surface deformation, structural analysis and design aspect of F6 subway station.

2 Statement of Problem

The development of infrastructures like underground structures in urban areas have been appeared the adjacent excavation problem, so the subway station construction are become a crucial platform for creating new topic in the current subject. In this paper, the interaction problem will be discussed in line 6 and 7 of Tehran metro project in Iran.

2.1 Project Overview

Tehran is the capital city of Iran with a population of around 9.4 million in the city and 15 million in the larger metropolitan area of Greater Tehran. Tehran metro line 6 and 7 projects have a length of about 39.5 km with 32 stations (named from A6-5 to Z6-1) and 32 km with 25 stations (named from A7 to Z7-3), respectively, Fig. 1. These lines have two exchange stations together (e.g. F6G7 and T7Q6 stations). The F6G7 subway station located at junction of 17th Shahrivar Street and Ghiam Street in ancient urban context of Tehran with lose ground conditions. In the current area, the link tunnel between these two lines placed near to F6 station (Fig. 1).

The tunnel of line 7 top of rail elevation is lower than the tunnel of line 6 top of rail elevation relative to ground surface in this area, so the link tunnel should be passed from lower elevation to higher one from line 7 tunnel to line 6 tunnel. The construction process of link tunnel makes the adjacent excavation problem to F6 subway station. The link tunnel has been driven in close proximity and beneath the F6 station based on Fig. 2 (see left figure). Figure 2 shows relative location of link tunnel near the F6 subway station in cross section as well as link

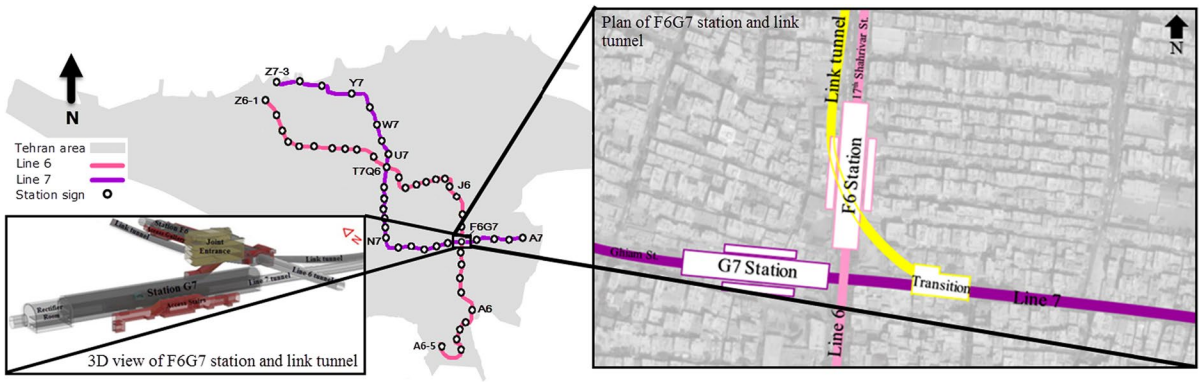

Fig. 1 Plan of line 6 and 7 of Tehran metro, F6G7 exchange subway station and link tunnel plan and 3D view

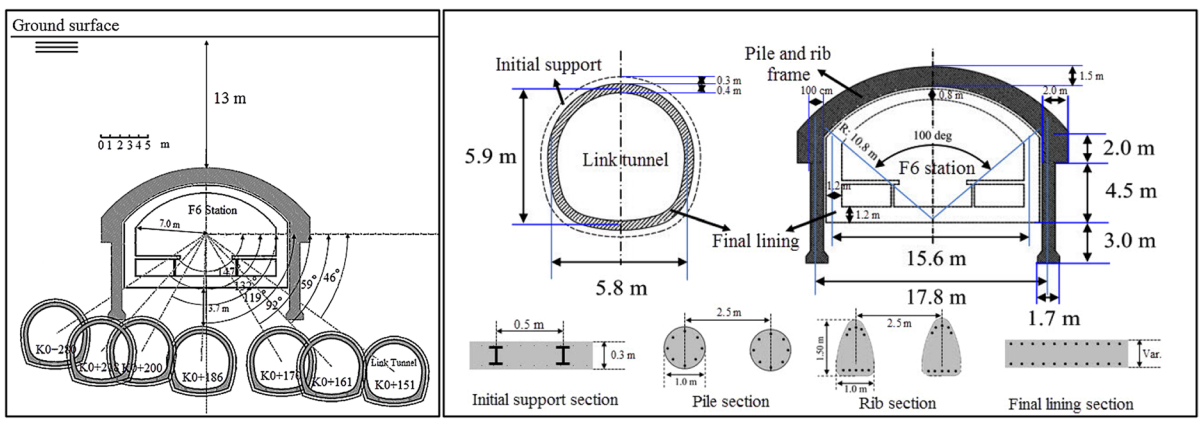

Fig. 2 F6 station and link tunnel relative location together (left figure) and their dimension and cross section (right figure)

tunnel and F6 subway station dimension. Link tunnel has a length of about 500 m that the overburden ranged from 30 to 18 m with the thickness of initial support and final lining of 30 and 40 cm, respectively (Fig. 2). Underground F6 station was located in depth of 13 m. The final lining thickness of station is ranged 80–120 cm (Fig. 2). Pile and rib system as a pre-supporting method was selected for construction of F6 station that will be discussed in the later paragraph. The ribs of station have half-oval cross-section of 100 cm width and 150 cm height and the piles have the diameter of 100 cm. Centrally distance between two set of pile and rib frames is 250 cm.

The most traditional and widespread Iranian technique for construction of large span underground spaces is Concrete Arch Pre-supporting System, (CAPS) including reinforced concrete arch elements or so-called ribs, each supported by piles at the two sides which all are constructed by manpower-excavation method prior excavating the main underground space (Sadaghiani and Dadizadeh 2010). The method was first introduced by Sadaghiani and Gheysar (2003) for construction of Mellat Station in 2002, which belongs line 2 of Tehran Metro in Iran.

In order to construct underground F6 subway station using CAPS technique, should be carried out in five steps. These steps of construction in cross sectional steps and 3D view are illustrated in Fig. 3 as follows:

Step 1—along the length of the station, an access gallery is excavated and multiple manually-excavated transverse access adits are made bilaterally from this gallery in certain distances to pile location. A longitudinal gallery is further manually-excavated at top of the rib along the length of the station and reinforced, whose vulgar name is *concreting gallery* (Fig. 3—Step 1),

Step 2—multiple wells are excavated in two sides of station to be used as piles. The piles get completed with reinforced concrete inside the wells (Fig. 3—Step 2),

Step 3—multiple manually-excavated curved adits with vulgar name of rib are made between bilateral piles. The ribs are concreted through concreting gallery (Fig. 3—Step 3),

Step 4—under the pile and rib pre-supporting system, it is possible to excavate the station cavern in large masses, so the excavation of station cavern is completed (Fig. 3—Step 4),

Step 5—the final lining of station is constructed (Fig. 3—Step 5).

2.2 Site Investigation and Geotechnical Study

Tehran is located on Quaternary alluvium according to the geological classification of Rieben at the foot of the Alborz Mountain Range that mainly consists of tuff, limestone, and dolomite (Rieben 1966). As a result, the non-uniform soil layers have been formed. To survey the geological and geotechnical characteristics of subsurface soil layers along F6 station, 4 Boreholes (BH) with maximum depth of 55.4 m were

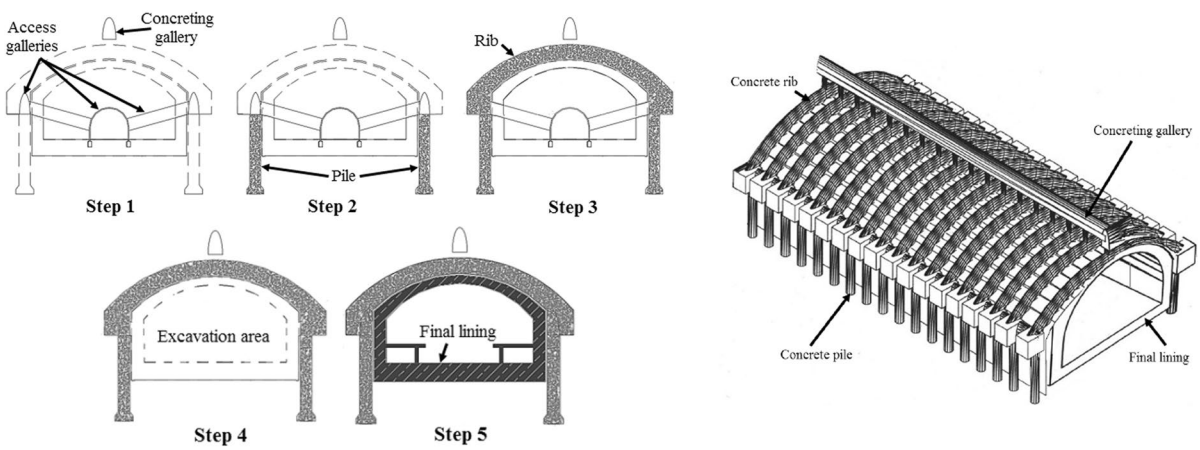

Fig. 3 Construction processes of CAPS technique (left figures) and 3D view (right figure) for underground F6 subway station

bored and a Test-Pit (TP) with 16 m depth was made too (Sahel Consulting Co., 2015). Typical engineering parameters measured by field and laboratory tests (e.g., SPT, PMT, DSHT, USCS, CU, etc.) to employing in numerical simulation.

The soil layers are composed of clayey SAND & GRAVEL, clayey SAND & sandy CLAY and also silty SAND & clayey GRAVEL. Figure 4 illustrates the longitudinal profile of geology and Ground Water Table (GWT) around F6 station. The geotechnical parameters of soil layers along the station are given in Table 1.

3 Numerical Simulation

A large range of geotechnical problems can be analyzed using numerical method. Finite element code as a worldwide numerical method is used for geotechnical applications and design purposes. Plaxis software is a finite element program, has been developed for the analysis of static elastoplastic deformation, stress states, stability, dynamics and groundwater flow in the field of geo-engineering and it covers most areas of tunnel engineering (Plaxis manual 2022). The numerical model consists of two crucial phases; model creation and model verification. The numerical simulation procedure with Plaxis 3D software that has been adopted for link tunnel-F6 station interaction problem are presented in Fig. 5. The numerical model consisted three phases that are defined in Fig. 5. Also, analytical and observational method were employed for validation and calibration the model that will be described in Sects. 3.2.1 and 3.2.2.

3.1 3D Finite Element Numerical Model

Geometry and mesh generation, applying initial and boundary conditions, the execution of calculation phase and the evaluation of the output results are the general procedures for a numerical model that were done in this paper. Numerical model assumptions and its properties in this study are as follows:

- The model is 160 m wide, it extended 200 m in y direction and it is 80 m deep (Fig. 6).
- Due to the distance of G7 station relative to F6 station and link tunnel, only the F6 station and

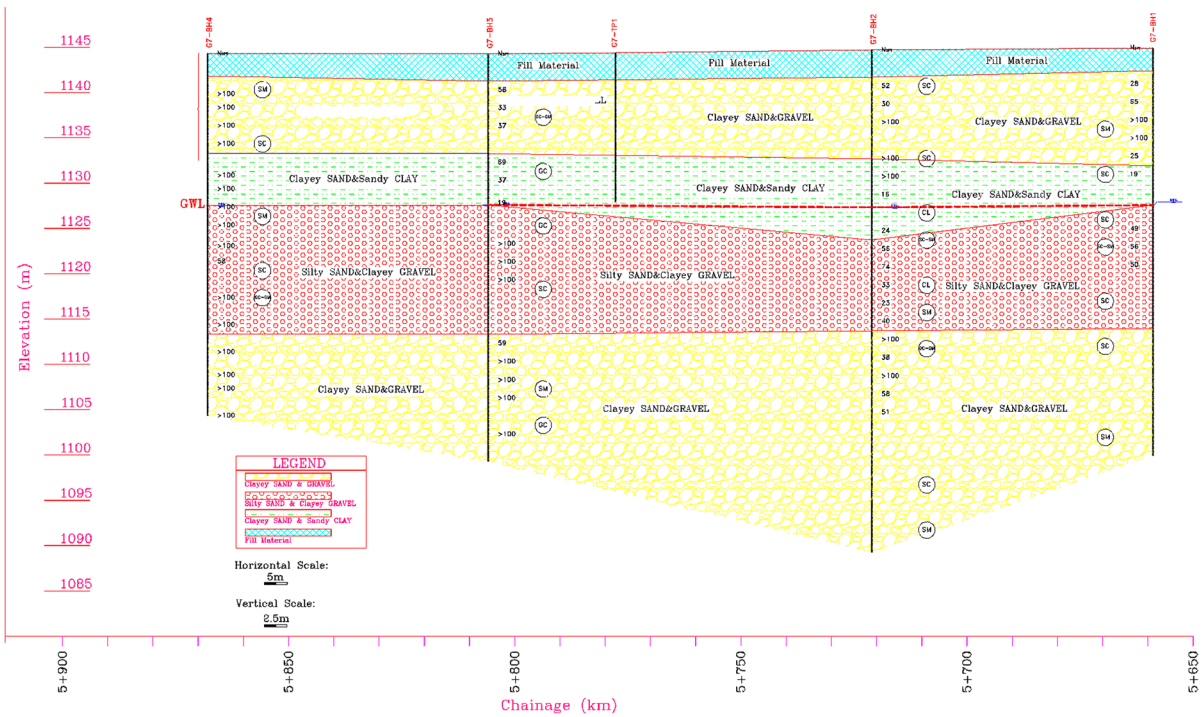

Fig. 4 Geotechnical longitudinal profile and ground water table along F6 Station and link tunnel

Table 1 Geotechnical parameters of soil layers

Layer No	Description	Depth (m)	γ_{unsat} KN/m^3	γ_{sat} KN/m^3	c' KN/m^2	ϕ' deg	ψ deg	K m/sec	K_0	E_{50}^{ref} KN/m^2	$E_{ur}^{ref}/E_{50}^{refa}$	$E_{ur}^{oed}/E_{50}^{refa}$
I	Man filled	0–2	19	–	20	20	–	–	0.66	1.5E4	3.0	1.0
II	GC/CM or SC	2–18	21	–	13	31	1	1E−04	0.48	6.5E4	3.0	1.0
III	SC/CL (Saturated)	> 18	20	22	25	28	–	5E−05	0.53	3.0E4	3.0	1.0

[a]As average values for various soil types, we have $E_{ur} \cong 3\ E_{50}$ and $E_{oed} = E_{50}$ (Plaxis manual 2022)

link structure as an interaction problem were considered in model (Fig. 6).

- The overburden and dimension of F6 station and link tunnel were model based on construction drawing (see Figs. 1, 2 and 6).
- The structural elements like concrete piles, concrete rib frames and tunnel lining were modeled as volume elements (clusters).
- The model consisted of 419,658 15-node hexagonal and 557,141 nodes, as well as the coarseness factor ranged 1–0.15.
- The model bottom boundaries, both in vertical and horizontal directions were set as fixed, as well as the lateral boundaries were set as fixed in the horizontal direction, whereas the top boundary was set free.
- The underground water has been accounted in level − 18 m from the ground surface.
- The traffic load and adjacent existing structures load are applied on ground surface of numerical model (20 Kpa).
- Considering the constitutive modeling, the soil layers were modeled as Hardening-Soil material. The hardening soil parameters were showed in Table 1. The Hardening-Soil model has been presented before as a hyperbolic model. Often hyperbolic soil models have been used to describe the nonlinear behavior. In contrast to an elastic perfectly-plastic model like Mohr–Coulomb, now the yield surface is not fixed but can expand due to plastic straining. However, soil stiffness in the Hardening-Soil model is described much more accurately using three different input stiffnesses: the triaxial loading stiffness, E_{50}, the triaxial unloading stiffness, E_{ur}, and the oedometer loading stiffness, E_{oed}.
- The nonlinear elastic behavior was adopted for structural elements by assigning the concrete properties to piles, ribs and lining.
- The soil mass around station were assumed as isotropic and homogenous.
- Characteristic compressive strength of shotcrete, initial structure and final lining were selected 15, 20 and 25 Mpa as a concrete structure.
- Elastic modules of concrete were calculated based on characteristic compressive strength of concrete.
- The unite weight of reinforced concrete structures was selected 25 kN/m^3.

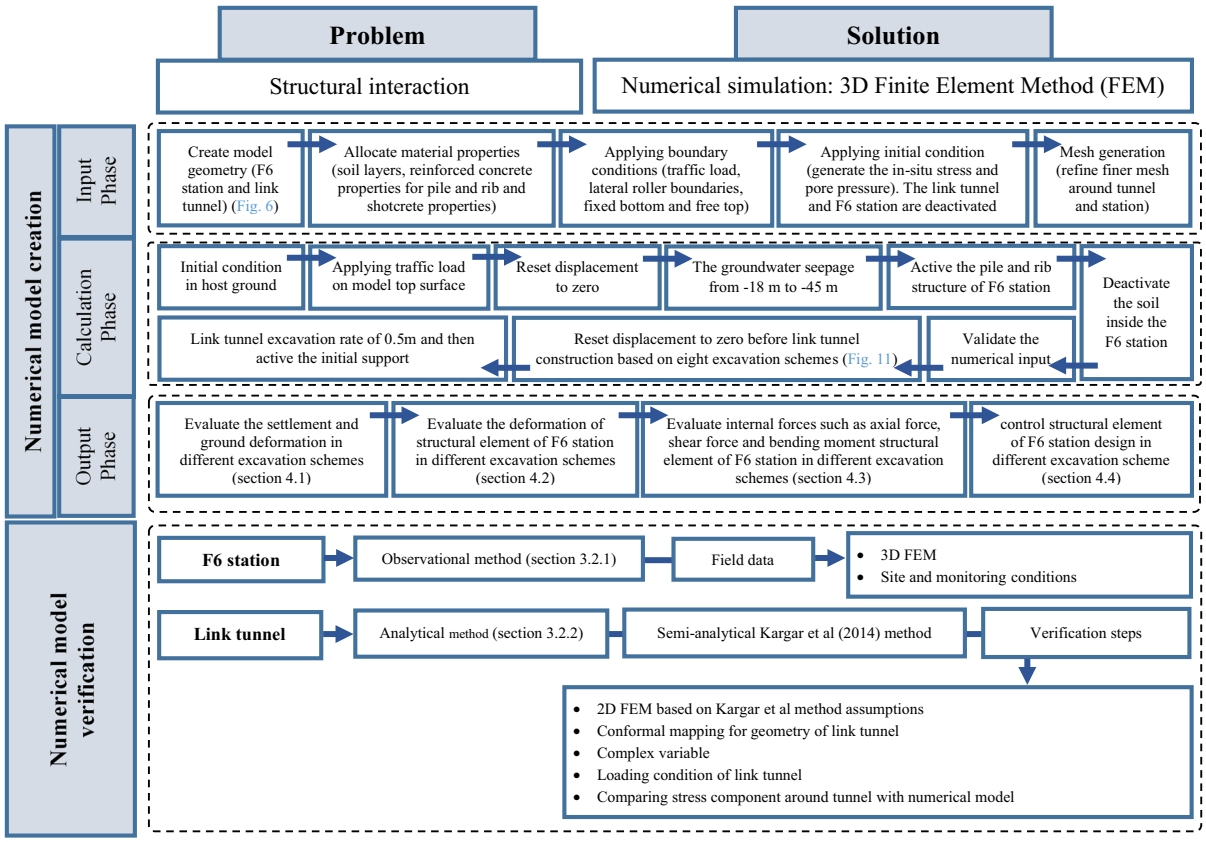

Fig. 5 Numerical simulation procedure for link tunnel–F6 station interaction analysis

- The groundwater seepage in project was done with drainage well, so the groundwater level reduction was modeled based on that condition.
- Over Consolidation Ratio (OCR) was selected 1 in all phases.
- The water level reduction settlement and F6 station construction settlement were set zero before link tunnel construction.
- The interface coefficient was selected 0.67 times of the cohesion and tangent of the internal friction angle.
- The soil lateral pressure (K_0) was calculated based on $K_0 = 1 - \sin\phi$ equation, ϕ is the internal friction angle (see Table 1).

3.2 Numerical Model Verification and Calibration

The semi-analytical method was employed for finite element model validation using 2D model. The analytical solutions have been used to validate the results of the numerical model (Kargar et al. 2014). Strength of material (thick-walled cylinder), Airy stress function and complex variable method are used as an analytical method for determining the stress field and deformation around a lined non-circular underground structure in elastic condition (Sadd 2009).

3.2.1 Analytical Method for Link Tunnel Model Verification

A semi-analytical elastic plain strain solution for stress field around a lined non-circular tunnel at great depth using complex variable method was introduced by Kargar et al. (2014). Owing to the link tunnel has non-circular geometric configuration, complex potential functions (Muskhelishvili and Kolosove's complex variable) and conformal mapping functions were used to determine stress component around tunnel

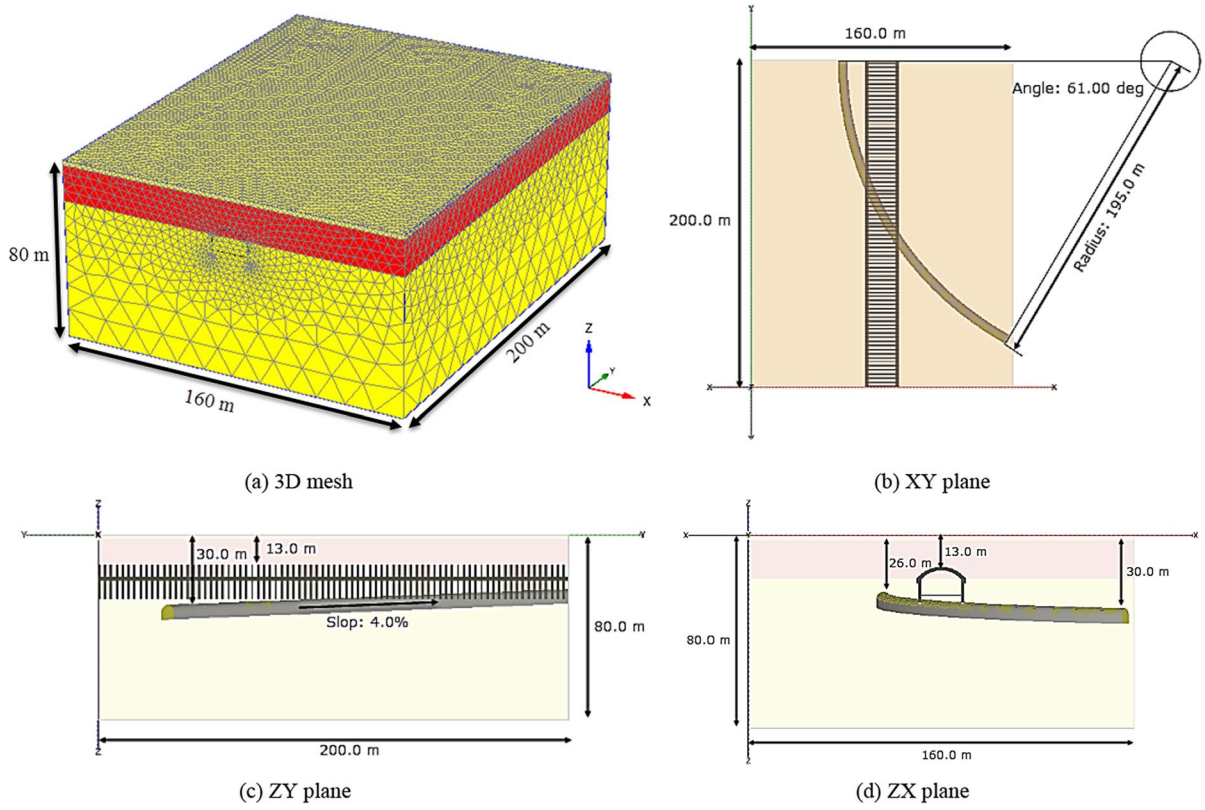

Fig. 6. 3D finite element model geometry and mesh generation

(Muskhelishvili and Radok 1953). Kargar method assumptions in the case of link tunnel are as follows:

- The link tunnel has a great overburden, e.g. 30 m, compared with the tunnel dimension, e.g. 5.9 m, so the tunnel considered in an infinite plane.
- The soil mass and concrete lining were assumed as isotropic, homogenous and liner elastic material.
- The initial liner was installed without any delay after tunnel excavation entirely.
- Due to the depth of tunnel, the tunnel subjected to a uniform stress state at infinity.
- There is a perfect adherence between liner and soil mass so that they have common deformation along the interface, therefore the soil-concrete interface has no-slip condition.

Based on Fig. 7, the infinite plane is divided into two zones named S_1 and S_2 that limited by contours L_1 and L_2. The regions S1 and S2 refer to soil mass and concrete lining with Young modulus E_1, E_2 and Poisson ratio ν_1, ν_2, respectively. Let $w(\xi)$ be a conformal mapping function which maps boundaries L_1 and L_2 into two concentric circles η_1 and η_2 with unit and R_0 radii. The function $w(\xi)$ thoroughly maps each exterior point of unit circle η_1 into region S_1 and each point in the region γ_2 bounded by circles η_1 and η_2 into region S_2 (Kargar et al 2014).

It is assumed that the conformal mapping function has the following expansion:

$$W(\xi) = Re^{i\frac{\pi}{2}}\left(\xi + \sum_{k=1}^{N} \omega_k \xi^{-k}\right), \quad (|\xi| \geq 1) \tag{1}$$

where $i = \sqrt{-1}$, R is a real constant affecting scale of the hole, ω_k is complex coefficient and $\pi/2$, is the angle by which the shape is rotated from its original position. Complex coefficient (ω_k) of Eq. (1) is computed by dividing the tunnel circumference into 15-degree angle (24 sectors) on z-plane (Fig. 7). The

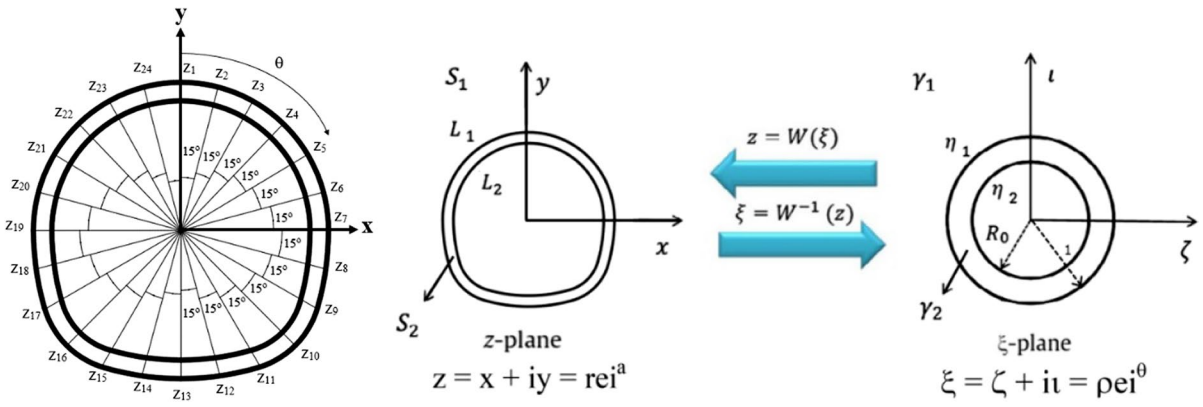

Fig. 7 Conformal mapping of link tunnel cross-section in z-plane into two concentric circles in ξ-plane

conformal mapping function coefficients (Eq. (2)) are given in Table 2.

$$\begin{aligned} Z &= x + iy = W(\xi) \\ &= 3.15e^{i\frac{\pi}{2}}(\xi + \omega_1\xi^{-1} + \omega_2\xi^{-2} \\ &\quad + \cdots + \omega_{24}\xi^{-24}), \quad (|\xi| \geq 1) \end{aligned} \tag{2}$$

According to semi-analytical Kargar et al. method, stress components could be determined for the region $|\xi| \geq 1$ from Muskhelishvili and Kolosove's complex variable as follows:

$$\begin{aligned} \sigma_r = \frac{1}{|\xi|^2 R\left(c_1'^2 + d_1'^2\right)} Re\Bigg\{ & \left(c_1' - id_1'\right)\sum_{j=1}^{n_1} j a_j \xi^{-j-1} \\ & + \left(c_1' + id_1'\right)\left(\frac{1}{t}\sum_{j=1}^{n_2} j\overline{d_j}\xi^{-j+1} + \mu_3\sum_{j=1}^{n-2} jT_j\xi^{j+1}\right) \\ & - \frac{G_1}{G_1 - G_2}\gamma Hi\sum_{j=1}^{n}\left(\frac{1+K}{2}\chi_{j,1} - \frac{1-K}{2}\omega_j\right)j\xi^{-j-1} \\ & - \left(\frac{\Gamma'\left(w'(\xi)\right)^2}{R}\right)\xi^2 + 2\frac{a_1'c_1' + b_1'd_1'}{R\left(c_1'^2 + d_1'^2\right)} + \Gamma\Bigg\} \end{aligned} \tag{3}$$

$$\begin{aligned} \sigma_\theta = -\frac{1}{|\xi|^2 R\left(c_1'^2 + d_1'^2\right)} Re\Bigg\{ & \left(c_1' - id_1'\right)\sum_{j=1}^{n_1} j a_j \xi^{-j-1} \\ & + \left(c_1' + id_1'\right)\left(\frac{1}{t}\sum_{j=1}^{n_2} j\overline{d_j}\xi^{-j+1} + \mu_3\sum_{j=1}^{n-2} jT_j\xi^{j+1}\right) \\ & - \frac{G_1}{G_1 - G_2}\gamma Hi\sum_{j=1}^{n}\left(\frac{1+K}{2}\chi_{j,1} - \frac{1-K}{2}\omega_j\right)j\xi^{-j-1} \\ & - \left(\frac{\Gamma'\left(w'(\xi)\right)^2}{R}\right)\xi^2 + 2\frac{a_1'c_1' + b_1'd_1'}{R\left(c_1'^2 + d_1'^2\right)} + \Gamma\Bigg\} \end{aligned} \tag{4}$$

$$\begin{aligned} \tau_{r\theta} = -\frac{1}{|\xi|^2 R\left(c_1'^2 + d_1'^2\right)} Im\Bigg\{ & \left(c_1' - id_1'\right)\sum_{j=1}^{n_1} j a_j \xi^{-j-1} \\ & + \left(c_1' + id_1'\right)\left(\frac{1}{t}\sum_{j=1}^{n_2} j\overline{d_j}\xi^{-j+1} + \mu_3\sum_{j=1}^{n-2} jT_j\xi^{j+1}\right) \\ & - \frac{G_1}{G_1 - G_2}\gamma Hi\sum_{j=1}^{n}\left(\frac{1+K}{2}\chi_{j,1} - \frac{1-K}{2}\omega_j\right)j\xi^{-j-1} \\ & - \left(\frac{\Gamma'\left(w'(\xi)\right)^2}{R}\right)\xi^2\Bigg\} \end{aligned} \tag{5}$$

where σ_r, σ_θ and $\tau_{r\theta}$ are radial, circumferential and tangential stress components, respectively. Furthermore, circumferential stress along circle η_1, from the side of the region γ_2 ($|\xi| = 1$), is calculated by Eq. (6). σ_r is calculated from Eq. (3) when $\xi = e^{i\theta}$. Obviously, circumferential stress along boundary L_2 could be obtained using Eq. (6) when $\sigma_r = 0$ and $\xi = R_0 e^{i\theta}$.

$$\sigma_\theta = 4\frac{c_1\prime a_2\prime + d_1\prime b_2\prime}{c_1'^2 + d_1'^2} - \sigma_r \tag{6}$$

where

$$\begin{aligned} a_1\prime &= Re\left\{ -\sum_{j=1}^{n_1} j a_j \xi^{-j-1} \right\}, b_1\prime = Im\left\{ -\sum_{j=1}^{n_1} j a_j \xi^{-j-1} \right\} \\ c_1\prime &= Re\left\{ \frac{w'(\xi)}{R} \right\}, d_1\prime = Im\left\{ \frac{w'(\xi)}{R} \right\} \end{aligned} \tag{7}$$

$$\begin{aligned} a_2\prime = Re\Bigg\{ & \sum_{j=1}^{n_2} j d_j \xi^{j-1} - s \sum_{j=1}^{n_1} j a_j \xi^{-j-1} \\ & + t\mu_3 \sum_{j=1}^{n-2} j\overline{T}_j \xi^{-j-1} - \frac{1}{1+k_2}\gamma HRi \\ & \times \sum_{j=1}^{n} \left(\frac{1-K}{2}\chi_{j,1} - \frac{1+K}{2}\omega_j \right) j\xi^{-j-1} \Bigg\} \end{aligned} \tag{8}$$

$$\begin{aligned} b_2\prime = Im\Bigg\{ & \sum_{j=1}^{n_2} j d_j \xi^{j-1} - s \sum_{j=1}^{n_1} j a_j \xi^{-j-1} \\ & + t\mu_3 \sum_{j=1}^{n-2} j\overline{T}_j \xi^{-j-1} - \frac{1}{1+k_2}\gamma HRi \\ & \times \sum_{j=1}^{n} \left(\frac{1-K}{2}\chi_{j,1} - \frac{1+K}{2}\omega_j \right) j\xi^{-j-1} \Bigg\} \end{aligned} \tag{9}$$

$$T_k = \begin{cases} \mu_{k+2} \sum_{j=1}^{n-(k+1)} j a_j q_{j+k+1}, & k > 0 \\ \mu_2 \sum_{j=1}^{n-1} j a_j q_{j+1}, & k = 0 \\ \sum_{j=0}^{n} (j-k-1) a_{j-k-1} q_j, & k < 0 \end{cases} \tag{10}$$

G_1 and G_2 are the shear modulus of soil mass and concrete liner, also K, H and γ are lateral coefficient pressure, tunnel overburden and stress gradient of soil mass, respectively. Functions $\chi_{i,k}$, μ_i and k_i are defined as follows:

$$\begin{aligned} \chi_{i,k} &= \begin{cases} 1 & i = k \\ 0 & i \neq k \end{cases}, \quad \mu_i = \begin{cases} 1 & i \leq n \\ 0 & i > n \end{cases} \\ k_i &= \begin{cases} 3 - 4_i & \textit{plane strain } (i = 1, 2) \\ \frac{3-_i}{1+_i} & \textit{plane stress } (i = 1, 2) \end{cases} \end{aligned} \tag{11}$$

a_i, d_i and q_i are unknow variables, as well as n_1 and n_2 are the number of terms for holomorphic functions

Table 2 Coefficients determined for conformal mapping function of link tunnel

R	R_0	ω_1	ω_2	ω_5	ω_{21}	ω_{22}	ω_{23}	ω_{24}
3.15	0.87	0.999	−0.018	−0.012	−0.012	0.014	−0.996	−0.012

**ω_3, ω_4 and ω_6 to ω_{20} are given zero

and n is the number of tunnel sectors. Γ and Γ' are real and complex constants with regard to stress state at infinity, which are determined as follows:

$$\begin{aligned} \Gamma &= \frac{1}{4}(\sigma_1+\sigma_2) = \frac{1+K}{4}\gamma H, \\ \Gamma\prime &= -\frac{1}{2}(\sigma_1-\sigma_2)e^{-2i\alpha} = -\frac{1-K}{2}\gamma H \end{aligned} \tag{12}$$

where σ_1 and σ_2 are principal stress components at infinity and α is the angel made between σ_1 direction and x axis and, respectively. t and s are the coefficient that defined by shear modules, plane strain and plane stress condition as follows:

$$t = \frac{G_1 - G_2}{G_1(1+k_2)}, \quad s = \frac{k_1 G_2 + G_1}{G_1(1+k_2)} \tag{13}$$

Here, the proposed semi-analytical solution by Kargar et al. (2014) is compared with Plaxis finite element result for link tunnel. Input data and loading data for link tunnel are represented in Tables 3 and 4, respectively.

The Eq. (14) was used for calculating the unknown variables a_i and d_i. The coefficients of Eq. (14) are introduced in Appendix A. Also, q_j, q'_j, $\overline{q}_j$, ι_j, ι'_j, β_j and β'_j were obtained by dividing the conjugate division of the coefficients of the conformal mapping function to the first derivative of the conformal mapping function. So, the Kargar et al. semi-analytical solution coefficient and unknown variable for link tunnel are presented in Tables 5 and 6, respectively.

$$\begin{bmatrix} [A_1]_{n_2\times n_1} & [A_2]_{n_2\times n_1} & [D_1]_{n_2\times n_2} & [D_2]_{n_2\times n_2} \\ [A\prime_1]_{n_1\times n_1} & [A\prime_2]_{n_1\times n_1} & [D\prime_1]_{n_1\times n_2} & [D\prime_2]_{n_1\times n_2} \end{bmatrix} \begin{bmatrix} [a]_{n_1\times 1} \\ [\overline{a}]_{n_1\times 1} \\ [d]_{n_2\times 1} \\ [\overline{d}]_{n_2\times 1} \end{bmatrix} = \begin{bmatrix} [B_1]_{n_2\times 1} \\ [B_2]_{n_1\times 1} \end{bmatrix} \tag{14}$$

Figure 8 shows magnitude of circumferential, radial and tangential stress components along soil mass and circumferential stress component along internal lining of link tunnel predicted by semi-analytical solution and Plaxis finite element software which indicates good agreement between numerical Plaxis model and semi-analytical Kargar et al. solution results. In brief, the results imply good accordance, proving the model validity and pave the way to apply the numerical model for analyzing different procedures of link tunnel construction. Due to the simplifications of semi-analytical elastic flat strain solution, there is difference of the radial stress components and the tangential stress components between two calculation methods.

3.2.2 *Observational Method for F6 Station Model Verification*

To verify the 3D model of F6 station model, field data measured during the F6 station construction were used. The station was constructed by CAPS method. Monitoring for surveying the settlement, includes topographic measurements for a network of benchmarks, some arranged on the axis and some transversely located to the route plan (7 benchmarks per cross section) as depicted in Fig. 9. The diagram depicted in Fig. 9, illustrates a layout which is an indicative of the benchmarks network on ground surface. Given the central station depth (H), monitoring instruments were installed transversely to the route at distances, 0.0H (exactly on axis), 0.5H, 1.0H and 1.5H away from axis. The longitudinal spacing for cross sections and plan, were set 0.5H. It's worthy to mention that the depth of the F6 station is 13.0 m.

The results of surface settlement acquired by numerical model and the monitoring system are rendered in Fig. 10. The results imply good accordance, proving the model validity and pave the way to apply the numerical model for analyzing.

4 Outcomes, Results and Discussions

The final choice of the method to be used for an underground opening construction in urban area depends upon the complex interaction of a number of factors such as safety, cost and schedule considerations, so engineering judgment is more effective than theoretical calculations (Hoek 2001). Selecting a suitable construction method for underground spaces is always among the key parameters for successful construction of the project (Sharifzadeh et al. 2013). Furthermore, choosing the support system and excavation sequences exert strong effects on the host ground stability and deformations. In this study, in order to find optimal excavation sequences for link tunnel, eight excavation schemes were proposed and numerically analyzed for excavation of link tunnel adjacent F6 station according to Fig. 11 as follows:

Table 3 Input data for link tunnel

Soil type	Elastic properties for soil			Elastic properties for concrete			Lateral pressure coefficient (K) K = 1 − sinϕ	Stress gradient (Mpa/m)	Overburden (m)	α (degree)
	E_1 (Mpa)	ν_1	G_1 (Mpa)	E_2 (Mpa)	ν_2	G_2 (Mpa)				
SC/CL	30	0.33	11.28	23,500	0.20	9792	0.53	0.02	30	π/2

Table 4 Loading data for link tunnel

σ_1 (Mpa)	σ_2 (Mpa)	Γ (Mpa)	Γ′ (Mpa)	k_1	k_2
− 0.6	− 0.318	0.2295	− 0.141	1.68	2.20

- Scheme “a”: full face excavation with curved invert in initial support system,
- Scheme “b”: full face excavation without any invert in initial support system,
- Scheme “c”: partial face excavation (top heading and bench) with curved invert in initial support system,
- Scheme “d”: partial face excavation (top heading and bench) without any invert in initial support system,
- Scheme “e”: pre-cutting method without any invert in initial support system,
- Scheme “f”: partial face excavation with top support core at the middle of tunnel without any invert in initial support system,
- Scheme “g”: partial face excavation with bench support core at the middle of tunnel without any invert in initial support system,
- Scheme “h”: partial face excavation with bench support core at the two sides of tunnel without any invert in initial support system.

The sequential number for ground material excavation and initial support installation are showed in Fig. 11. The schemes “c” to “h” are selected based on Sequential Excavation Method (SEM). SEM tunnelling is determined by a sequential removal of host ground followed by the installation of initial support. The ground deformation, structural deformation and internal forces of structural elements of F6 station are the important factors for selecting the proper excavation schemes for link tunnel adjacent F6 station. During the selection of excavation sequences, main factors such as number of excavation stages, subdividing area, pre-supporting system, core support and ring closure time were considered. The advance rate was selected 0.5 m and trailing distance between different faces were simulated at distances of 12 m (2*T.D.) based on U.S. FHWA (2009).

Table 5 Kargar et al. coefficients for link tunnel

n1	n2	n	g	t	υ	s	λ
10	40	24	271.96	− 270.96	− 455.06	456.06	184.09

Table 6 Kargar et al. unknown variables for link tunnel

j	β_j	β'_j	ι_j	ι'_j	q_j	q'_j	a_j	d_j
0	–	–	–	–	0.220564	219.6699	–	–
1	− 1.18 + 0.13i	− 1.09 + 0.20i	− 252.9 − 543.9i	− 2.08 − 73.5i	0.549265	− 196.294	0.4 + 3i	4 + 0.5i
2	− 1.18—0.13i	− 1.09—0.20i	− 252.9 + 543.9i	− 2.08 + 73.5i	0.240575	131.5302	4—0.5i	− 6i
3	− 1.09 + 0.41i	− 1.55 + 1.91i	46.4 − 89.9i	12.31 − 8.1i	− 0.73027	− 277.492	− 0.1 − 0.5i	− 0.99
4	− 1.09—0.41i	− 1.55 − 1.91i	46.4 + 89.9i	12.31 + 8.1i	0.240921	93.7976	0.9	− 0.21
5	− 0.92 + 0.66i	− 0.12 + 0.22i	1.05 − 21.6i	8.05 − 1.7i	− 0.76662	− 222.562	− 0.7 + 7i	− 0.3
6	− 0.92 − 0.66i	− 0.12 − 0.22i	1.05 + 21.6i	8.05 + 1.7i	0.228013	67.04162	0.6 + 1i	− 6 + 3i
7	− 0.70 + 0.87i	− 0.71 + 0.83i	− 6.18 − 5.34i	− 0.98 − 6.44i	− 0.68635	− 178.834	− 0.2 + 4i	− 0.14
8	− 0.70—0.87i	− 0.71—0.83i	− 6.18 + 5.34i	− 0.98 + 6.44i	0.212135	47.07069	0.1	0.91
9	− 0.44 + 1.02i	− 0.78 + 4.02i	− 4.80 + 1.41i	− 7.33 + 7.8i	− 0.72995	− 144.002	0.4i	0.14i
10	− 0.44 − 1.02i	− 0.78 − 4.02i	− 4.80 − 1.41i	− 7.3 − 7.8i	0.192873	32.26093	0.2i	0.6 − 1i
11	1.18 + 0.14i	2.56 + 3.76i	271.5 − 382.7i	9.5 − 382.7i	− 0.77787	− 116.186	–	0.1i
12	1.18 − 0.14i	2.56 − 3.76i	271.5 + 382.7i	9.5 + 382.7i	0.169797	21.36966	–	7.2i
13	1.09 + 0.41i	5.79 + 0.09i	− 30.78 − 100.2i	− 8.7 − 7.66	− 0.83035	− 93.9028	–	33.1i
14	1.09 − 0.41i	5.79 − 0.09i	− 30.78 + 100.2i	− 8.7 + 7.66i	0.142474	13.4453	–	7 + 1i
15	0.93 + 0.66i	2.65 + 1.45i	− 0.32 − 24.2i	− 0.12 − 4.1i	− 0.88759	− 75.9996	–	47i
16	0.93 − 0.66i	2.65 − 1.45i	− 0.32 + 24.2i	− 0.12 + 4.1i	0.110792	7.784133	–	3i
17	0.71 + 0.87i	6.65 + 0.47i	6.50 − 6.32i	1.50 − 6.32i	− 0.94624	− 61.3451	–	− 0.96i
18	0.71 − 0.87i	6.65 − 0.47i	6.50 + 6.32i	1.50 + 6.32i	0.074785	3.834874	–	5 + 0.2i
19	0.44 + 1.02i	0.21 + 1.02i	5.30 + 0.91i	0.4 + 0.391i	− 1.00564	− 49.377	–	1 + 0.1i
20	0.44 − 1.02i	0.21 − 1.02i	5.30 − 0.91i	0.4 − 0.391i	0.037866	1.314971	–	1 − 0.1i
21	0.15 + 1.10i	0.33 + 1.40i	2.11 + 3.82i	54.3 + 0.43i	− 1.00657	− 37.4176	–	7 + 1i
22	0.15 − 1.10i	0.33 − 1.40i	2.11 − 3.82i	54.3 − 0.43i	0.002012	− 0.1704	–	44i
23	− 0.15 + 1.10i	− 0.50 + 1.30i	− 1.50 + 3.99i	− 1.54 + 0.9i	− 0.996	− 28.171	–	1i
24	− 0.15 − 1.10i	− 0.50 − 1.30i	− 1.50 − 3.99i	− 1.54 − 0.9i	− 0.012	− 0.39011	–	43
25	− 0.01	− 0.04	− 1.17	− 1.45	–	–	–	5i
26	–	–	–	–	–	–	–	0.1 + ii
27	–	–	–	–	–	–	–	0.2i
28	–	–	–	–	–	–	–	1.9i
29	–	–	–	–	–	–	–	− 1 + 0.1i
30	–	–	–	–	–	–	–	9.07i
31	–	–	–	–	–	–	–	0.4 + 1i
32	–	–	–	–	–	–	–	0.3i
33	–	–	–	–	–	–	–	14
34	–	–	–	–	–	–	–	0.21
35	–	–	–	–	–	–	–	0.44i
36	–	–	–	–	–	–	–	0.44i
37	–	–	–	–	–	–	–	0.8i
38	–	–	–	–	–	–	–	0.76
39	–	–	–	–	–	–	–	0.1i
40	–	–	–	–	–	–	–	0.6i

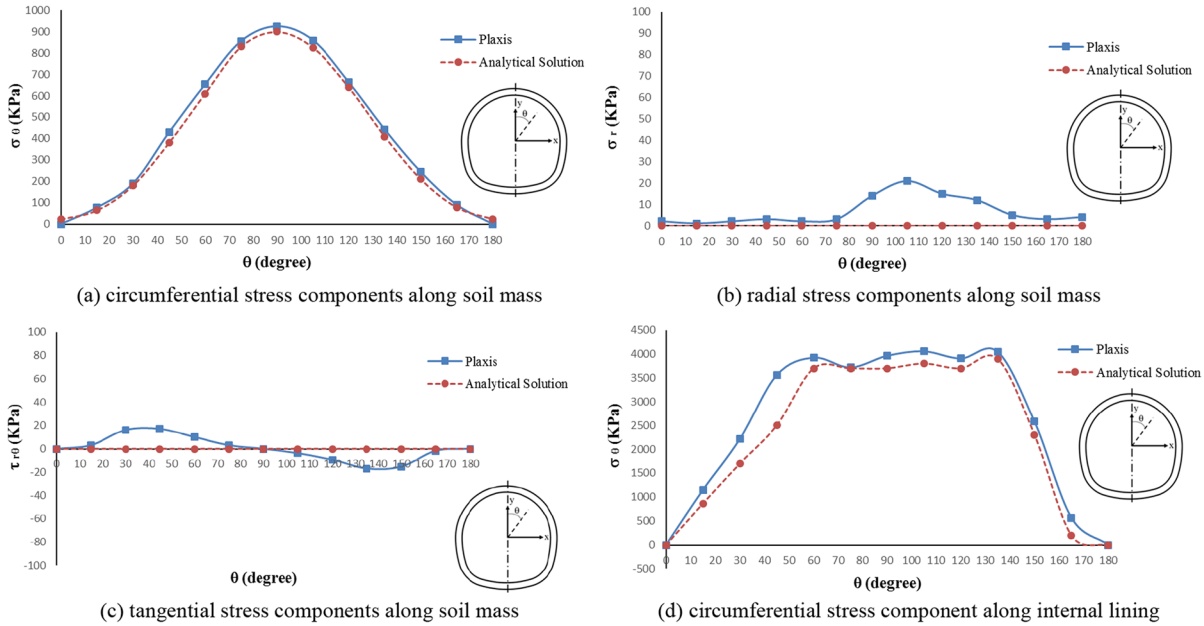

Fig. 8 Stress distribution along soil mass and internal lining of link tunnel predicted by Kargar et al. (2014) method and Plaxis software

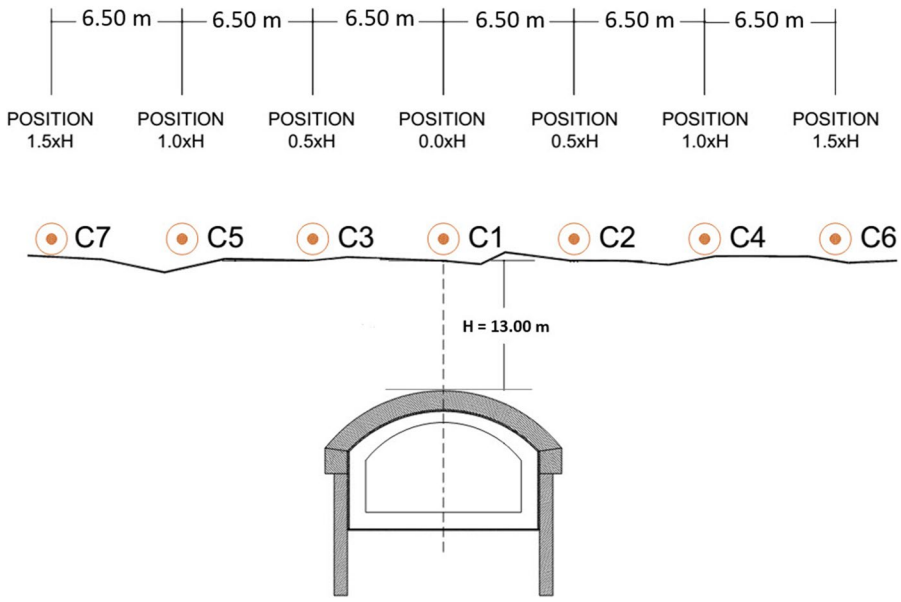

Fig. 9 Layout of benchmarks in cross section around F6 station

4.1 Settlement and Ground Deformation

Based on Fig. 5, the link tunnel was constructed with different schemes according to Fig. 11 after construction of F6 station using pile and rib method, in other words, the link tunnel is excavated under existed F6 station that constructed by pile and rib method as a pre-supporting system. Four different sections were selected based on Fig. 12 to monitor the ground deformation and structural forces as follows:

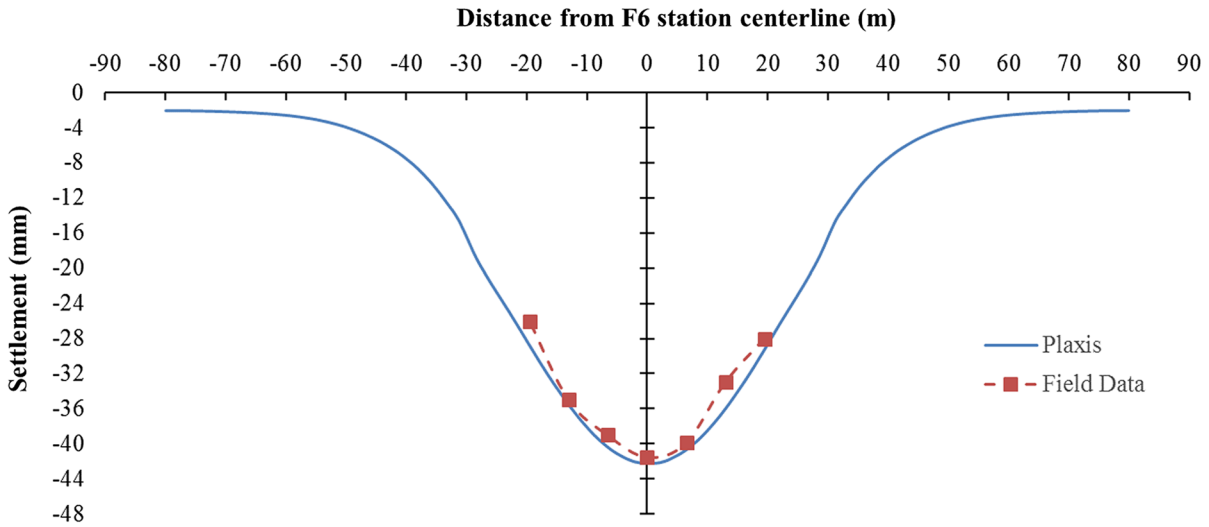

Fig. 10 The result of the surface settlement in numerical model and field measurement of F6 station

- Section 1: the location of rib No. 70 (at the distance of 27 m from start point of link tunnel excavation),
- Section 2: the location of rib No. 50 (at the distance of 57 m from start point of link tunnel excavation),
- Section 3: the location of rib No. 41 (at the distance of 100 m from start point of link tunnel excavation),
- Section 4: the location of rib No. 32 (at the distance of 123 m from start point of link tunnel excavation).

Transverse surface settlement profiles for eight excavation sequences are illustrated in Figs. 13 for section 1, 2, 3 and 4 based on Fig. 12. Based on Fig. 13, the minimum and maximum surface settlement value were calculated over the tunnel centerline for "c" and "b" excavation schemes, respectively. The "e" and "c" excavation schemes have the same trend in some sections. Figure 14 shows the minimum to maximum surface settlement classification for the proposed excavation schemes (Fig. 11) for the link tunnel. Based on the numerical modeling results, the partial excavation method ("c" excavation scheme),

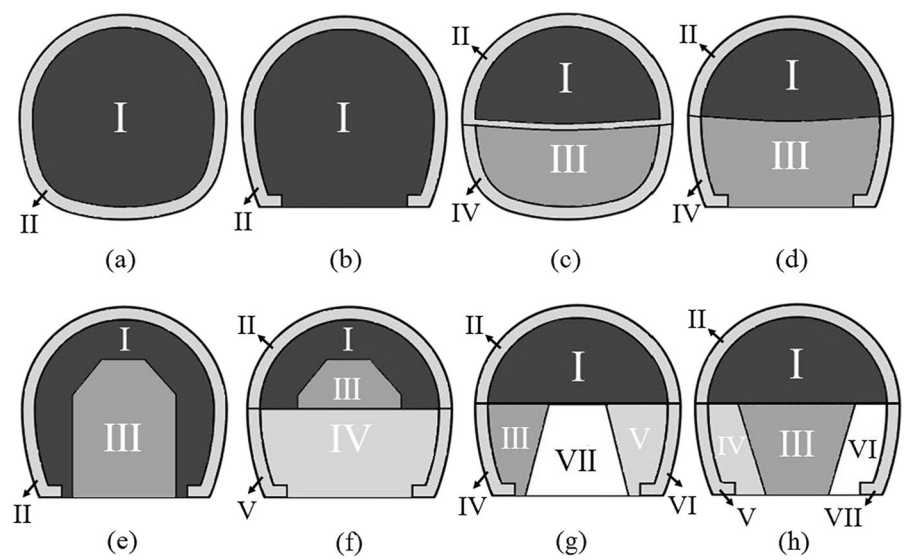

Fig. 11 Proposed excavation schemes for link tunnel adjacent to F6 station

curved invert installation that make oval shape for tunnel ("c" and "a" excavation schemes) and pre-supporting techniques like pre-cutting method ("e" excavation scheme) can reduce the ground deformation.

The location of link tunnel relative to F6 station has a direct effect on surface settlement profile, for example, the maximum and minimum surface settlement based on proposed excavation schemes are about 60.9 and 39.2 mm in section 3—rib No. 41 (Fig. 13c), respectively, however the maximum and minimum surface settlement are about 79.0 and 49.7 mm in section 2—rib No. 50 (Fig. 13b), respectively. In brief, the link tunnel are located right under the pile and rib frame in section 3 itself, but in section 1, 2 and 4, the link tunnel are placed left or right side of the F6 station, as a result, in the former case shows lower surface settlement than later cases.

The longitudinal displacement profiles along the link tunnel centerline based on eight proposed excavation schemes are seen in Fig. 15, also, the intersection area of F6 station and link tunnel is clearly illustrated in this figure. Based on Fig. 15, among eight proposed schemes, the "c" scheme is proper excavation scheme, based on their potential for limitation the ground deformation. Based on empirical relation that have been given by Attewell and Woodman (1982), the ratio of the surface settlement above the tunnel face to the final settlement, (i.e., $S_v/S_{v,\ max}$), is almost 50%. This result is in excellent agreement with Attewell and Woodman (1982) study based on Fig. 15.

4.2 Deformation of Structural Elements

In the theory of structures, when a deformation occurs in a structural member, the internal forces such as axial force, shear force, bending moment and torsion are created within it. In this research, the link tunnel excavation induces the deformation to the host ground of F6 station, as a result, it causes additional internal forces in pile and rib system of F6 station. This ground deformation sometimes disrupts the stability and capacity of structures with the sign of the crack, rupture and local instabilities in the structural element. In order to characteristic the deformation of structural element of F6 station (e.g. concrete pile and rib), the rib and pile deformation are presented due to the link tunnel excavation for "c" and "b" excavation schemes in Figs. 16 and 17, respectively. It goes

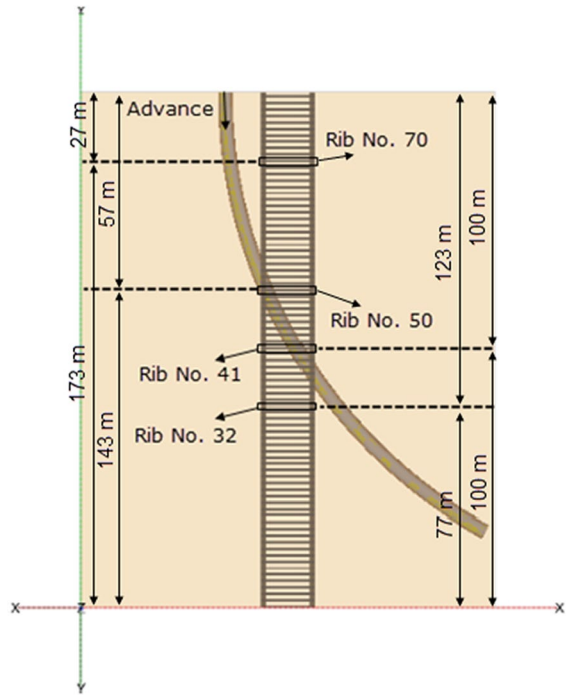

Fig. 12 Monitoring section in the location of ribs No. 70, 50, 41 and 32

without saying that the "c" excavation scheme and "b" excavation scheme show minimum and maximum surface settlement, respectively.

According to Fig. 16, the location of link tunnel relative to F6 station shows different rib deformation, for example, in section 1 and 2 (Fig. 16a, b), the left side of rib that the link tunnel existed there, illustrates more deformation than other side. Based on Fig. 17, the pile deformation is totally vertical deformation due to the reduced of pile bearing capacity. Table 7 shows the rib deformation after link tunnel excavation for "b" and "c" excavation schemes.

Based on Fig. 16 and Table 7, the rib deformation and its differential displacement in section 3 (rib No. 41) are less than other section because the link tunnel are located right beneath the F6 station, in this condition the stiffness of soil mass around link tunnel comes up, however in section 2 (rib No. 50), more deformation induces due to the location of link tunnel relative to F6 station. Rib No. 32 and 70 deformation are placed in second and third place after rib No. 41 because of more rib deformation.

According to the numerical modeling results in Fig. 17, the farther distance of link tunnel relative

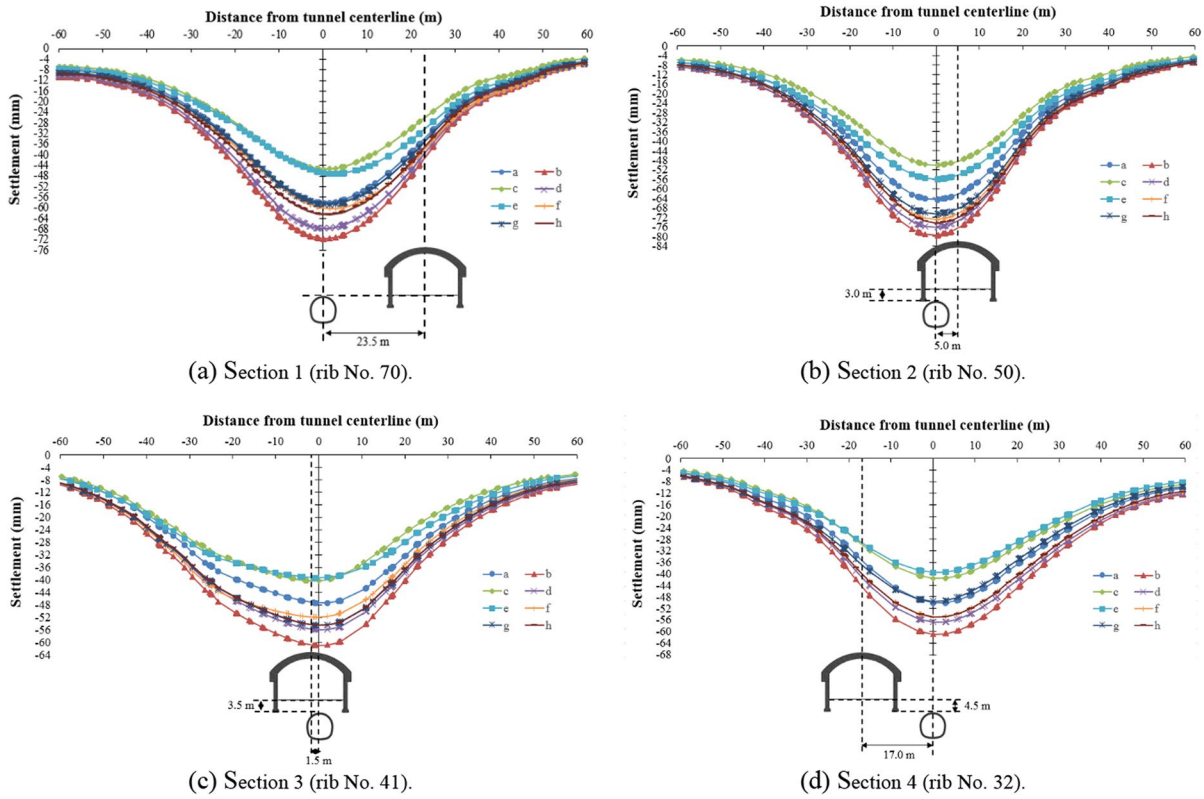

(a) Section 1 (rib No. 70). (b) Section 2 (rib No. 50).

(c) Section 3 (rib No. 41). (d) Section 4 (rib No. 32).

Fig. 13 Transverse settlement profiles for the proposed excavation schemes (in Fig. 11) for the link tunnel

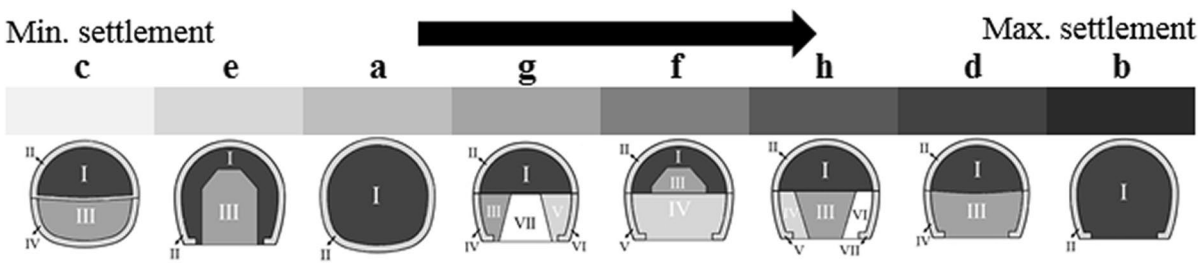

Fig. 14 Minimum to maximum surface settlement value classification for the proposed excavation schemes (in Fig. 11) for the link tunnel

to station piles shows less deformation in pile, for instance when the distance between link tunnel and F6 station centrally is 23.5 and 5 m, the left pile deformation is illustrated 56 and 87.7 mm in "b" excavation scheme, respectively. However, the differential displacement between left and right piles decreased when the link tunnel located right under the pile and rib frame, in this condition the stiffness of soil mass around link tunnel comes up.

4.3 Analysis of Structural Elements

The variation of bending moment in ribs No. 32, 41, 50 and 70 of F6 station before and after link tunnel excavation for "b" and "c" excavation schemes are demonstrated in Fig. 18. In the rib No. 50 (Fig. 18b), the maximum negative bending moment is changed from 310 ton.m before link tunnel excavation to 524 ton.m after link tunnel excavation using "b"

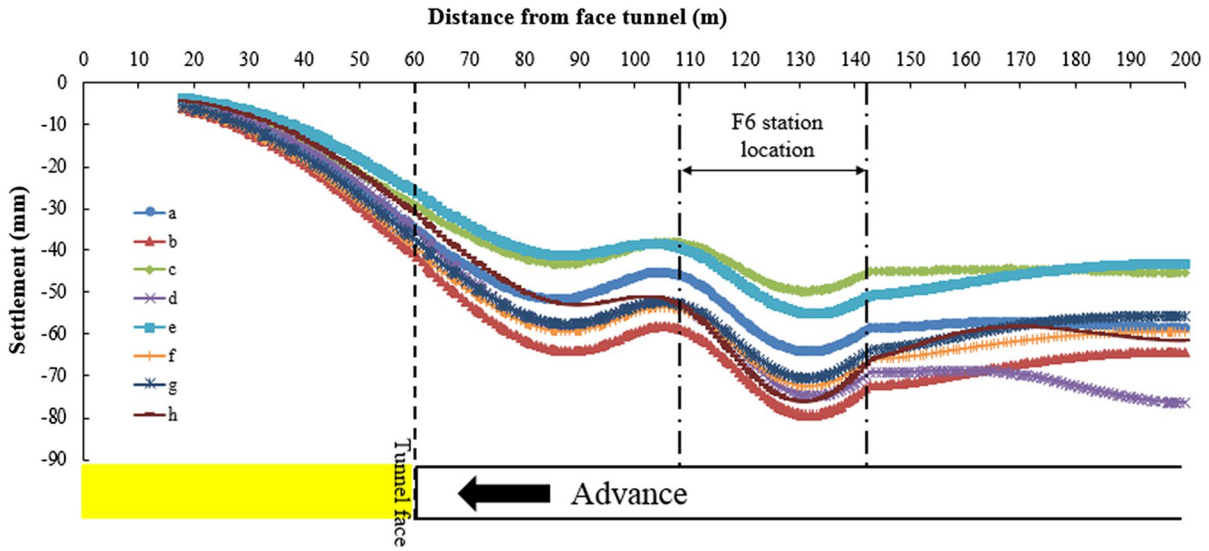

Fig. 15 Longitudinal displacement profiles for the proposed excavation schemes (in Fig. 11) for the link tunnel

excavation scheme. The farther distance of link tunnel relative to station induces less amount of bending moment in ribs. The variation of shear force in ribs No. 32, 41, 50 and 70 of F6 station before link tunnel excavation and after link tunnel excavation for "b" and "c" excavation schemes are demonstrated in Fig. 19. Shear force changes more in the rib-pile connection than elsewhere. In general, the shear force increases uniformly along the entire length of the rib. The variation of axial force in ribs No. 32, 41, 50 and 70 of F6 station before link tunnel excavation and after link tunnel excavation for "b" and "c" excavation schemes are demonstrated in Fig. 20. Axial force amount can be increased or decreased depending on the position of the link tunnel relative to the station. The axial compressive force in rib No. 50 (Fig. 20b) is increased from 612 to 815 ton after link tunnel excavation using "b" excavation scheme. The variation of bending moment, shear force and axial force in left and right piles No. 32, 41, 50 and 70 of F6 station before link tunnel excavation and after link tunnel excavation for "b" and "c" excavation schemes are demonstrated in Figs. 21, 22 and 23, respectively.

The negative bending moment of piles are changed more than positive bending moment after link tunnel construction, Fig. 21. According to Fig. 22, the shear forces of piles are not changed noticeable except in the pile-rib connection. The shear force is a critical force in concrete elements like CAPS, so the concrete element rupture is predicted in pile-rib connection. By excavating the link tunnel near the left pile of F6 station, the bearing capacity of this pile, as a result axial force are decreased, and then the axial force is redistributed in right piles based on Fig. 23.

4.4 Design Control of Structural Elements

The concrete pile and rib were designed by ACI 318-14 design code (ACI Committee 318, 2014), so the critical load combination for concrete pile and rib should be plotted inside axial force—bending moment interaction diagram of pile and rib. Figure 24 shows the critical load combination based on ACI 318-14 design code and axial force—bending moment interaction diagram for pile and rib, the critical point of load combination should be marked inside the interaction diagram. According to the design results of pile and rib, the structural capacity of pile and rib are not adequate after link tunnel excavation for "b" scheme, however for "c" excavation scheme is adequate. The proper excavation scheme for link tunnel can ensure the safety of F6 underground subway station.

The shear capacity of pile and rib elements are computed by ACI 318-14 design code (ACI Committee 318, 2014). Shear capacity of piles and ribs ranged 111–123 and 115–125 ton/m, respectively. The induced shear force in pile and rib after link

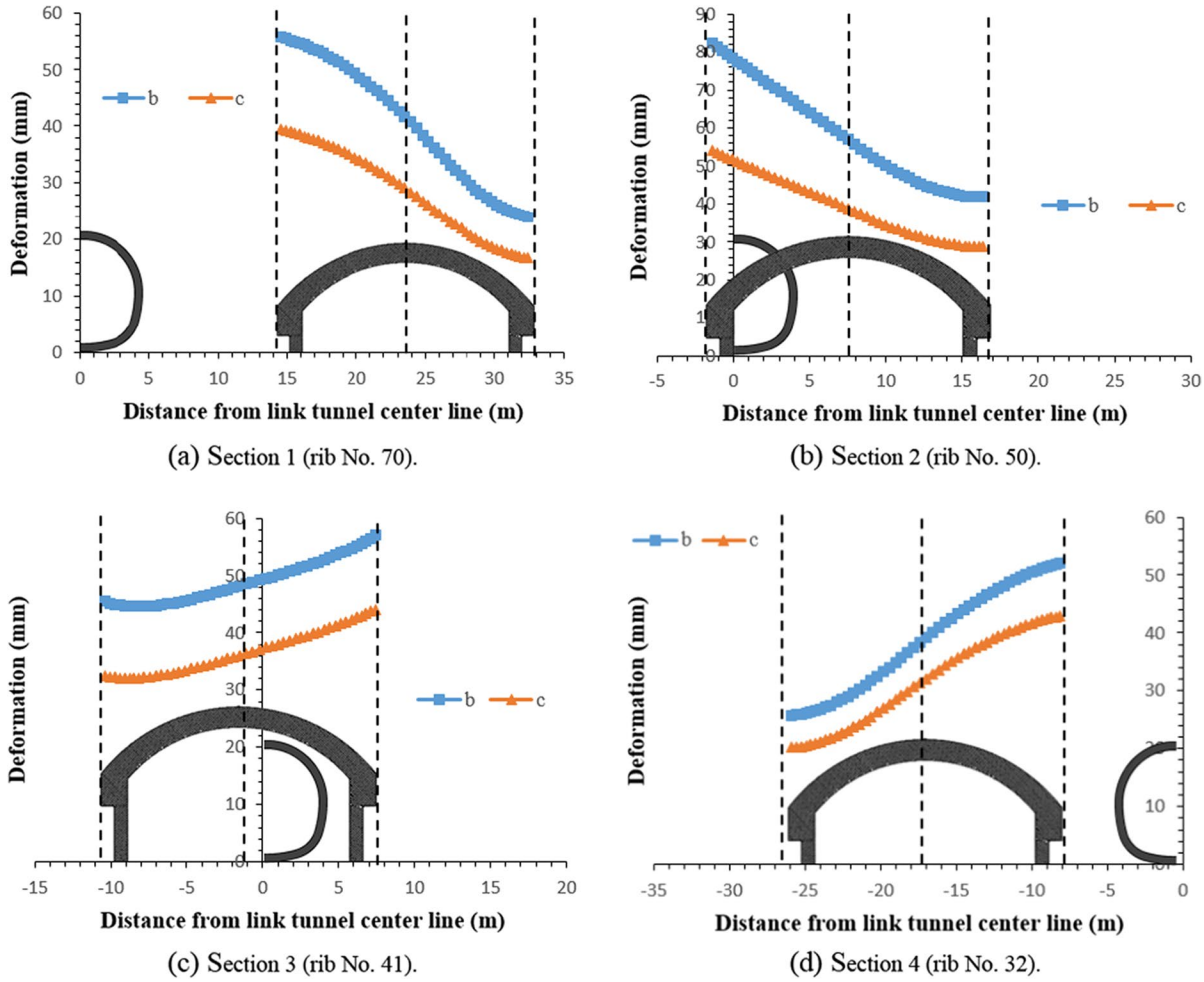

Fig. 16 Rib deformation profiles for excavation schemes (**b**) and (**c**) for the link tunnel

excavation in "b" and "c" schemes exceeded than shear capacity of pile and rib. The axial force—bending moment interaction capacity of pile and rib for "c" excavation scheme are adequate, but the shear capacity is not adequate. There is suggested that the final lining of F6 station be build first and then the link tunnel constructed.

5 Conclusion

The study focuses on intersection area of line 6 and 7 of Tehran metro in Iran which placed F6G7 exchange subway station and link tunnel. The link tunnel are constructed adjacent main structure of F6 exchange subway station construction. The construction process of link tunnel makes the adjacent excavation problem to F6 subway station. The aim of the paper is to study the interaction problem of existed underground F6 subway station and link tunnel using numerical model, analytical and observational method. The proper excavation scheme for link tunnel can ensure the safety of F6 underground subway station. The most significant results are given below:

1. The minimum and maximum surface settlement value were calculated over the tunnel centerline for "partial face excavation with curved invert" and "full face excavation without any invert" excavation schemes for link tunnel, respectively, based on numerical model in Fig. 14.

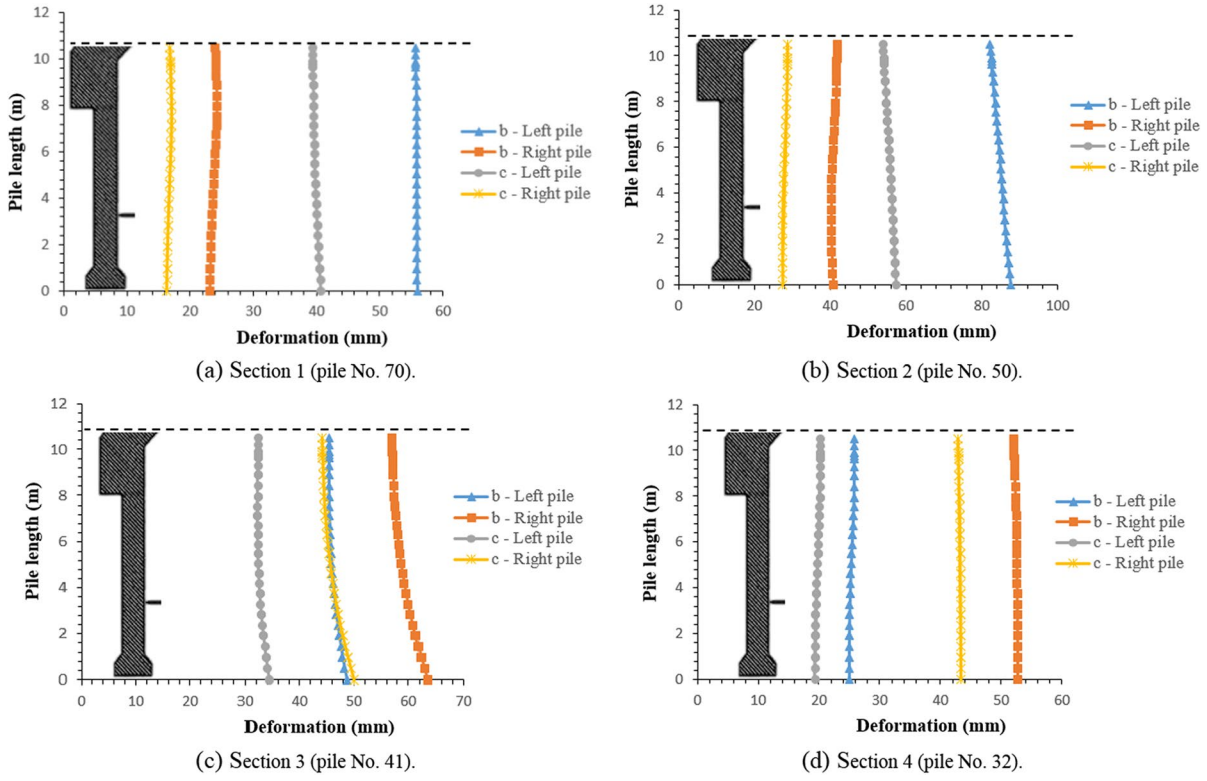

Fig. 17 Pile deformation profiles for excavation schemes (**b**) and (**c**) for the link tunnel

Table 7 Rib deformation after link tunnel excavation for (b) and (c) excavation scheme

Rib No	(b) Excavation scheme			(c) Ecavation scheme		
	Deformation (mm)		Δd (mm)	Deformation (mm)		Δd (mm)
	Max	Min		Max	Min	
70	55	24	31	39	17	22
50	81	42	39	53	29	24
41	57	45	12	44	32	12
32	52	26	26	43	21	22

2. The core support in the tunnel face, invert installation and pre-cutting method as a pre-supporting technique have significant influence on surface settlement in this case. The partial excavation method by considering the above conditions can reduce the ground deformation based on Fig. 13.
3. By excavating the link tunnel near each pile of F6 station, the bearing capacity of this pile, as a result axial force are decreased, and then the axial force is redistributed in other piles. There is suggested that the final lining of F6 station is build first and then the link tunnel constructed.

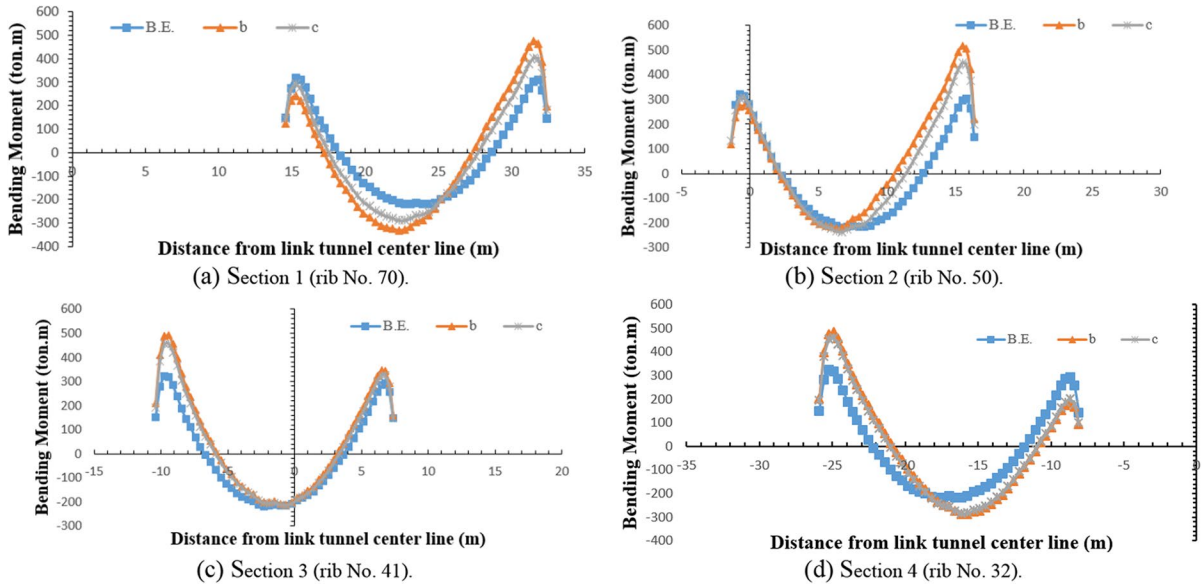

Fig. 18 Variation of bending moment in ribs before link tunnel excavation and after excavation schemes (**b**) and (**c**) for the link tunnel

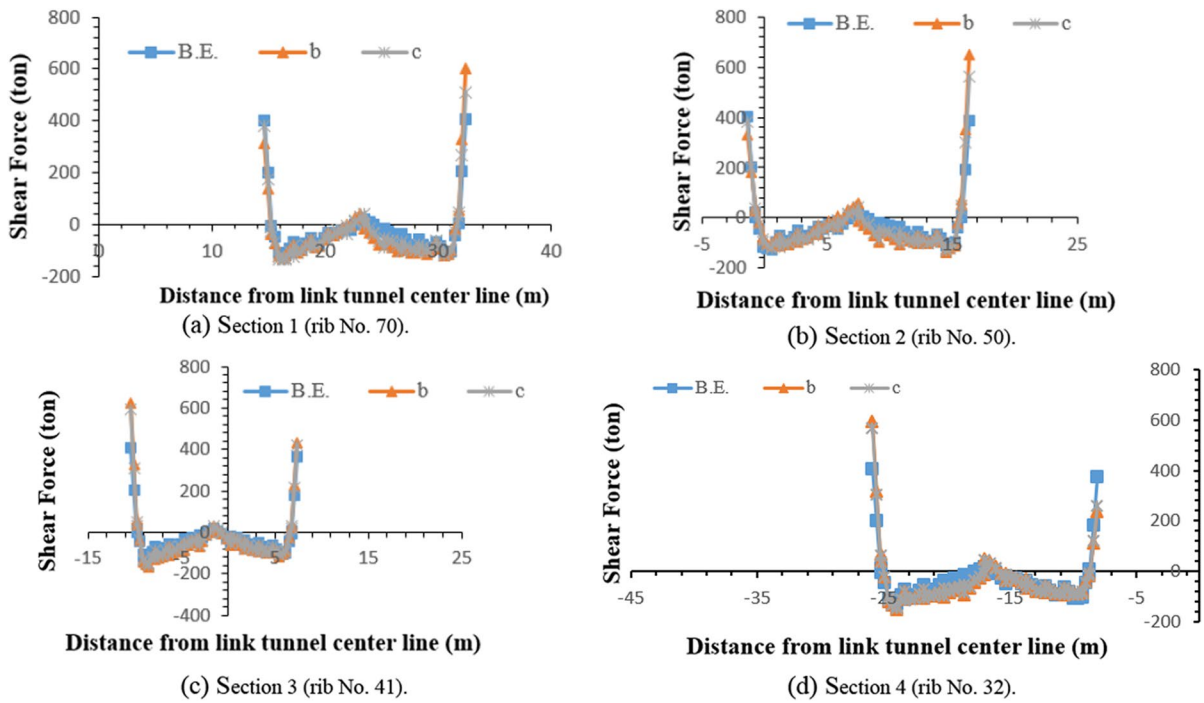

Fig. 19 Variation of shear force in ribs before link tunnel excavation and after excavation schemes (**b**) and (**c**) for the link tunnel

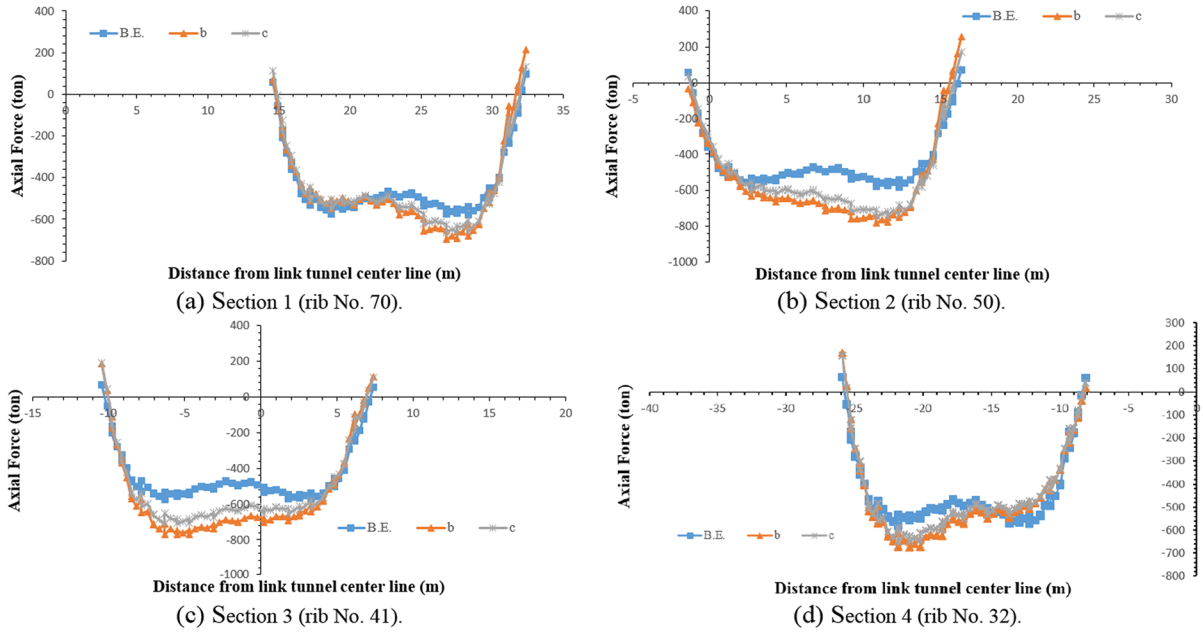

(a) Section 1 (rib No. 70). (b) Section 2 (rib No. 50). (c) Section 3 (rib No. 41). (d) Section 4 (rib No. 32).

Fig. 20 Variation of axial force in ribs before link tunnel excavation and after excavation schemes (**b**) and (**c**) for the link tunnel

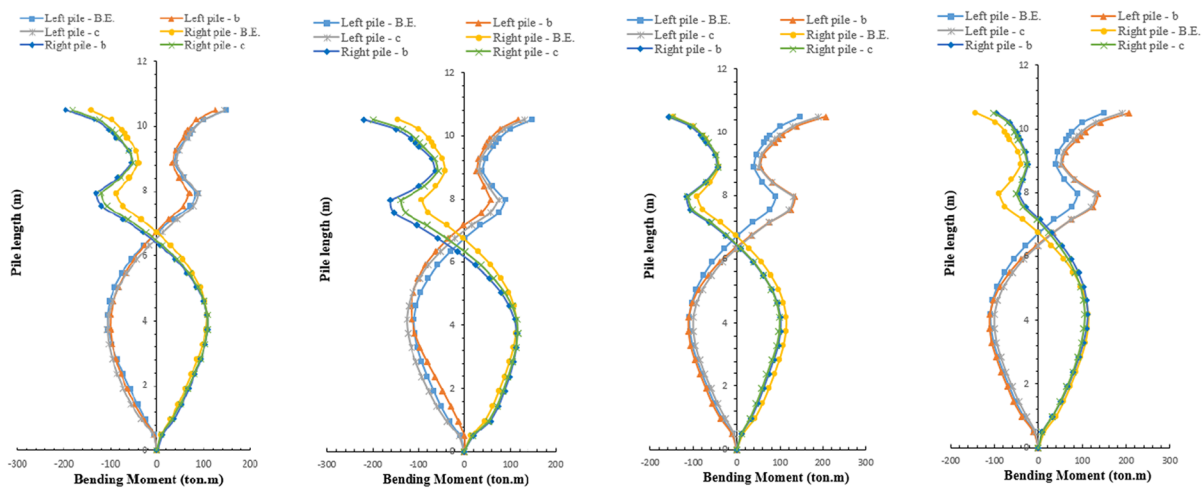

(a) Section 1 (pile No. 70). (b) Section 2 (pile No. 50). (c) Section 3 (pile No. 41). (d) Section 4 (pile No. 32).

Fig. 21 Variation of bending moment in piles before link tunnel excavation and after excavation schemes (**b**) and (**c**) for the link tunnel

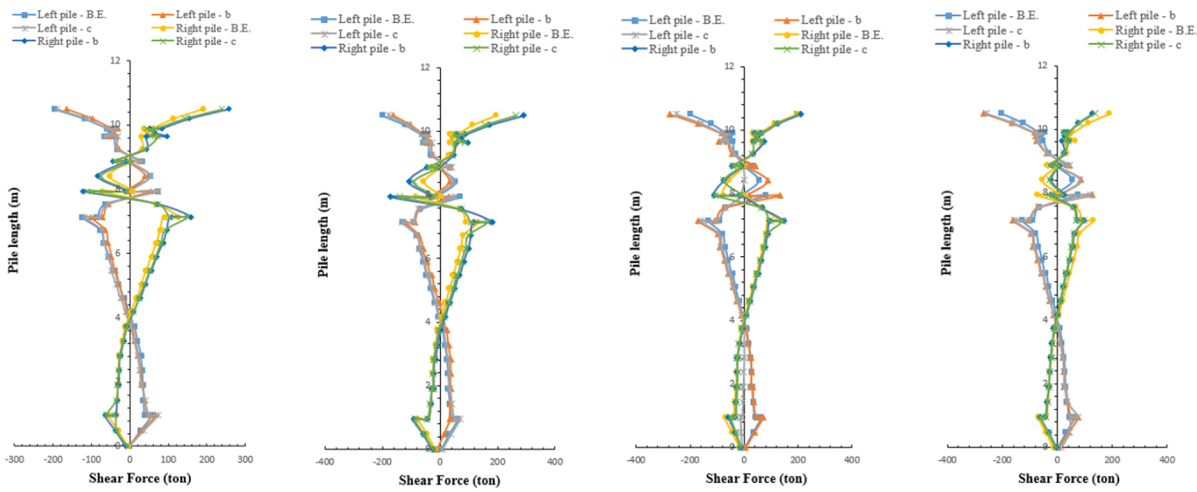

(a) Section 1 (pile No. 70). (b) Section 2 (pile No. 50). (c) Section 3 (pile No. 41). (d) Section 4 (pile No. 32).

Fig. 22 Variation of shear force in piles before link tunnel excavation and after excavation schemes (**b**) and (**c**) for the link tunnel

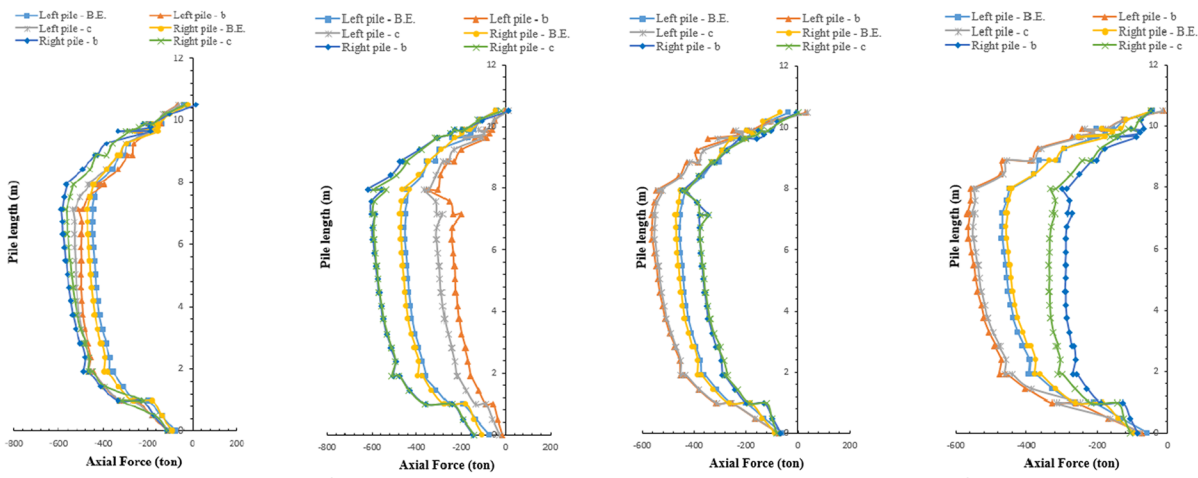

(a) Section 1 (pile No. 70). (b) Section 2 (pile No. 50). (c) Section 3 (pile No. 41). (d) Section 4 (pile No. 32).

Fig. 23 Variation of axial force in piles before link tunnel excavation and after excavation schemes (**b**) and (**c**) for the link tunnel

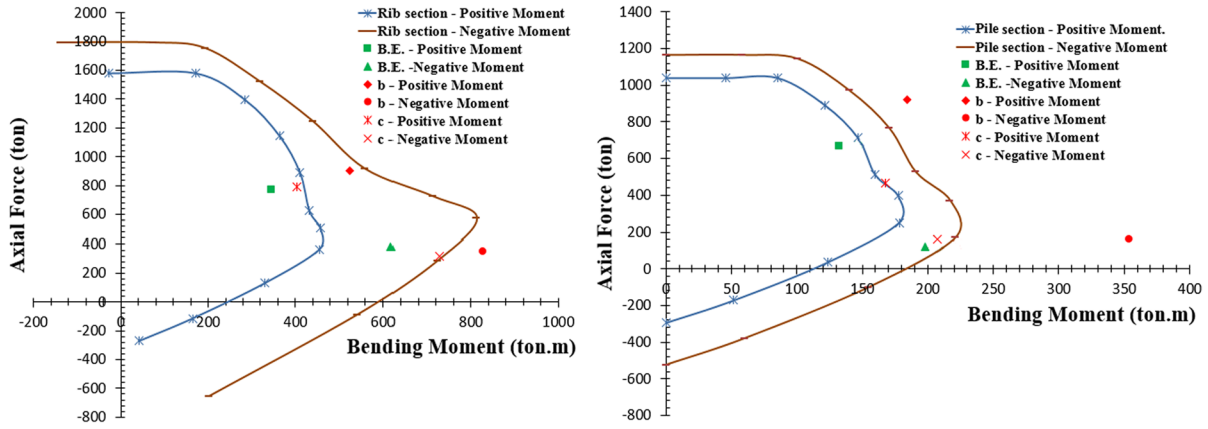

Fig. 24 Axial force—bending moment interaction diagram for pile (left figure) and rib (right figure)

Acknowledgements Authors would like to dedicate their special thanks to Amirkabir University of Technology (Tehran Polytechnic) for their valuable efforts and cooperation to let authors get access to software and facilities for the study, as well as Dr Alireza Kargar, Assistant Professor of Rock Mechanics in Tehran University for his guidance in analytical method section and Mr. Mohammad Askari for his guidance to use MATLAB software. The authors also express their gratitude to the Tehran Urban and Suburban Railway Company (TUSRC) for granting aid and allowance to authors to get access to the required data needed for the research completion.

Funding This research received no specific grant from any funding agency in the public, commercial, or not-for-profit sectors.

Data Availability Data available on request from the authors under d.mohammadi@aut.ac.ir.

Declarations

Conflict of interest The authors declare that they have no known competing financial interests or personal relationships that could have appeared to influence the work reported in this paper.

Appendix A

Coefficients of equation set (14) are presented as follows:

$$A_{1m,k} = kR_0^{-m}s(\mu_{k-m+n+2}C'''_{m-k-1} + \mu_{k-m+1}\mu_{n+m-k-1}(q_{k-m+1} - R_0^{-(k-m+1)}q'_{k-m+1})) \tag{A1}$$

$$A_{2m,k} = kR_0^{-m} \times \left(t\mu_3\mu_{m+k}\sum_{j=m-1}^{n-(k+1)} j(R_0^{-(j-m+1)}q'_{j-m+1} - q_{j-m+1}) \times \overline{q}_{j+k+1} - t\mu_3\mu_{n+3-p}\sum_{j=1}^{p-2}\mu_{j+k+1}jC'''_{m-j-1}\overline{q}_{k+j+1} \right) \tag{A2}$$

$$D_{1m,k} = -kR_0^{-m+1}\sum_{j=1}^{n+1}\beta_j^{k+m-2}(R_0^{-1}\iota_j - \iota'_j) \tag{A3}$$

$$D_{2m,k} = \chi_{m,k}(R_0^m + \frac{g}{t}R_0^{-m}) \tag{A4}$$

$$A'_{1m,k} = -kR_0^m(-\lambda q_{m+k+1}\mu_{k+m+1} + sR_0^{-(k+m+1)}\mu_{k+m+1}q'_{k+m+1} + tR_0^{-2m}\mu_{k+m+1}q_{k+m+1}) \tag{A5}$$

$$A'_{2m,k} = \chi_{m,k}(sR_0^{-m} + \upsilon R_0^m) + kt\mu_{m+2}R_0^m \sum_{j=1}^{n-(m+1)}\mu_{j+k+1}j(R_0^{-(j+m+1)}q'_{j+m+1} - q_{j+m+1})\overline{q}_{j+k+1} \tag{A6}$$

$$D'_{1m,k} = k(\mu_{k+2n-m-1}R_0^{k-1}q''_{m-k+1} - R_0^{m+1}\sum_{j=1}^{n+1}\beta_j^{k-m-2}(R_0^{-1}\iota_j - \iota'_j)) \tag{A7}$$

$$D'_{2m,k} = 0 \tag{A8}$$

$$\begin{aligned} B_{1m} = {} & \frac{1}{1+k_2}(C''_{-m}\mu_{j-1} + \gamma HRi(-\frac{1-K}{2}R_0^{-m}C^*_{m-2}\mu_{3-m+n} \\ & + \frac{1+K}{2}\sum_{j=1}^{m-2}j\omega_j R_0^{-m}\mu_j C^*_{m-j-1})) - \frac{1}{1+k_2}(R_0^{-m}C'_{-m}\mu_{j-1} \\ & + \gamma HRi(\frac{1-K}{2}R_0^{-m}C^{**}_{m-2-1}\mu_{3-m+n} - \frac{1+K}{2}\sum_{j=1}^{m-2}j\omega_j C^{**}_{m-j-1}R_0^{-m}\mu_j)) \\ & + \gamma HRR_0^{-m}i(\frac{k_2}{1+k_2} - \frac{gG_1}{G_1-G_2})(-\frac{1+K}{2}\chi_{m,1} + \frac{1-K}{2}\omega_m)\mu_m \end{aligned} \tag{A9}$$

$$\begin{aligned} B_{2m} = {} & \gamma HR\mu_m i\frac{k_2R_0^m + R_0^{-m}}{1+k_2}(-\frac{1+K}{2}\omega_m \\ & + \frac{1-K}{2}\chi_{m,1}) - \frac{\mu_{m+2}}{1+k_2}(C'_m R_0^m - C''_m) \end{aligned} \tag{A10}$$

Coefficients q''_k, C'_k, C''_k, C'''_k, C^*_k and C^{**}_k are determined as follows:

$$q''_k = \begin{cases} \frac{R_0^{n+1}q''_{k-n-1} - \sum_{j=1}^{n-1}j\omega_j R_0^{n-j}q''_{k+j-n}}{n\omega_n} & k > 2n+1 \\ \frac{\omega_n R_0^{n+1}(R_0^{-n} - R_0^n) + R_0^{n+1}q''_n - \sum_{j=1}^{n-1}j\omega_j R_0^{n-j}q''_{n+j+1}}{n\omega_n} & k = 2n+1 \\ \frac{\omega_{k-n-1}\left(R_0^{-(k-n-1)} - R_0^{(k-n-1)}\right)R_0^{n+1} - \sum_{j=1}^{k-n}(n-j)\omega_{n-j}R_0^j q''_{k-j}}{n\omega_n} & n+1 < k \le 2n \\ -\frac{(n-1)\omega_{n-1}q''_n R_0}{n\omega_n} & k = n+1 \\ R_0^{n+1}\frac{R_0 - R_0^{-1}}{n\omega_n} & k = n \\ 0 & k < n \end{cases} \tag{A11}$$

$$C_k\prime = \begin{cases} \gamma HRi(q_{k+2}\frac{1-K}{2} - \frac{1+K}{2}\sum_{J=k+2}^{n}(j-k-1)\omega_{j-k-1}q_j)\mu_{k+2} & k \ge 0 \\ \gamma HRi(q_1\frac{1-K}{2} - \frac{1+K}{2}\sum_{j=1}^{n}j\omega_j q_j) & k = -1 \\ \gamma HRi(q_0\frac{1-K}{2}\chi_{-k,2} - \frac{1+K}{2}\sum_{j=-(k+1)}^{n}j\omega_j q_{j+k+1})\mu_{-(k+1)}\mu_{k+2+n} & k < -1 \end{cases} \tag{A12}$$

$$C''_k = \begin{cases} \gamma HRi(q_{k+2}\prime R_0^{-2}\frac{1-K}{2} - \frac{1+K}{2}\sum_{J=k+2}^{n}(j-k-1)\omega_{j-k-1}R_0^{k-j}q_j\prime)\mu_{k+2} & k \ge 0 \\ \gamma HRi(q_1\prime R_0^{-2}\frac{1-K}{2} - \frac{1+K}{2}\sum_{j=1}^{n}j\omega_j R_0^{-(j+1)}q_j\prime) & k = -1 \\ \gamma HRi(q_1\prime R_0^{-2}\frac{1-K}{2}\chi_{-k,2} - \frac{1+K}{2}\sum_{j=-(k+1)}^{n}j\omega_j R_0^{-(j+1)}q_{j+k+1}\prime)\mu_{-(k+1)}\mu_{k+2+n} & k < -1 \end{cases} \tag{A13}$$

$$C'''_k = -R_0\sum_{j=1}^{n+1}\beta_j^{k-1}(R_0^{-1}\iota_j - \iota_j\prime) \tag{A14}$$

$$C^*_k = R_0\sum_{j=1}^{n+1}\beta_j^{k-1}\iota_j\prime \tag{A15}$$

$$C_k^{**} = -\sum_{j=1}^{n+1} \beta_j^{k-1} \iota_j \tag{A16}$$

where $g = \frac{k_2 G_1 + G_2}{G_1(1+k_2)}$, $t = \frac{G_1 - G_2}{G_1(1+k_2)}$, $\upsilon = \frac{k_2 G_1 + k_1 G_2}{G_1(1+k_2)}$, $s = \frac{k_1 G_2 + G_1}{G_1(1+k_2)}$, $\lambda = \frac{(1-k_2)G_1 - (1-k_1)G_2}{G_1(1+k_2)}$ and $p = Min(m, n)$.

References

ACI Committee 318 (2014) Building code requirements and for reinforced concrete (ACI318-14) commentary (318R-89). Detroit: American Concrete Institute.

Asano T, Ishihara M, Kiyota Y, Kurosawa H, Ebisu S (2003) An observational excavation control method for adjacent mountain tunnels. Tunn Undergr Space Technol 18:291–301

Attewell PB, Woodman JP (1982) Predicting the dynamics of ground settlement and its derivitives caused by tunnelling in soil. Ground Eng 15(7):13–22, 36

Chakeri H, Hasanpour R, Hindistan MA, Ünver B (2011) Analysis of interaction between tunnels in soft ground by 3D numerical modeling. Bull Eng Geol Environ 70(3):439–448

Ding Z, Zhang M, Zhang X, Wei X (2023) Theoretical analysis on the deformation of existing tunnel caused by undercrossing of large-diameter slurry shield considering construction factors. J Tunneling Undergr Space Technol 133. https://doi.org/10.1016/j.tust.2022.104913

Eslami B, Golshani A (2017) Performance of CAPS method considering its interaction with adjacent structures—the Q7 station of Tehran Metro Line 7. Int J Geoeng Case Histories 4(3):147–161

Fang Q, Tai Q, Zhang D, Wong LNY (2016) Ground surface settlements due to construction of closely-spaced twin tunnels with different geometric arrangements. Tunn Undergr Space Technol J 51:144–151

Franzius JN (2003) Behaviour of buildings due to tunnel induced subsidence. PhD thesis, Department of Civil and Environmental Engineering of Imperial College of Science, Technology and Medicine London, pp 21–22

Hoek E (2001) Big tunnel in bad rock. J Geotech Geoenviron Eng 127(9):726–740

Hosseini S, Shahriar K, Monjezi M, Jannesari A (2011) 3D numerical model of large span and intersection tunnel, case study: line 3 and 7 Tehran metro. First Asian and 9th Iranian tunneling symposium

Huang Z, Zhang H, Long Z, Qiu W, Meng G, Zhu L (2021) Field test optimization of shield tunnelling parameters undercrossing an existing high-speed railway tunnel: a case study. J Geotech Geol Eng 39:1381–1398. https://doi.org/10.1007/s10706-020-01564-3

Jin D, Yuan D, Li X, Zheng H (2018) An in-tunnel grouting protection method for excavating twin tunnels beneath an existing tunnel. Tunn Undergr Space Technol 71:27–35

Kargar AR, Rahmannejad R, Hajabasi MA (2014) A semi-analytical elastic solution for stress field of lined non-circular tunnels at great depth using complex variable method. Int J Solids Struct 51:1475–1482

Kim SH, Burd HJ, Milligan GWE (1996) Model testing of closely spaced tunnels in clay. Géotechnique 48(3):375–388

Klar A, Vorster TEB, Soga K, Mair RJ (2005) Soil—pipe interaction due to tunnelling: comparison between Winkler and elastic continuum solutions. Géotechnique 55(6):461–466

Klar A, Vorster TE, Soga K, Mair RJ (2007) Elastoplastic solution for soil-pipe-tunnel interaction. J Geotech Geoenviron Eng 133(7):782–792

Li XG, Yuan DJ (2012) Response of a double-decked metro tunnel to shield driving of twin closely under-crossing tunnels. Tunn Undergr Space Technol J 28:18–30

Liang R, Xia T, Hong Y, Yu F (2016) Effects of above-crossing tunnelling on the existing shield tunnels. Tunn Undergr Space Technol J 58:159–176

Liu HY, Small JC, Carter JP, Williams DJ (2009) Effects of tunnelling on existing support systems of perpendicularly crossing tunnels. Comput Geotech 36(5):880–894

Liu Z, Xue J, Ye J, Qian J (2021) A simplified two-stage method to estimate the settlement and bending moment of upper tunnel considering the interaction of undercrossing twin tunnels. Transp Geotech 29

Mohammadi D, Shahriar K, Parsapour D (2021) Interaction of excavated tunnels by earth pressure balance machines and sub-surface obstacles; case study: Tehran metro line 7. J Min Environ 12(3):799–814. https://doi.org/10.22044/jme.2021.10868.2061

Muskhelishvili NI, Radok JRM (1953) Some basic problems of the mathematical theory of elasticity. Cambridge Univ Press, Cambridge

Ng CW, Lee KM, Tang DK (2004) Three-dimensional numerical investigations of new Austrian tunnelling method (NATM) twin tunnel interactions. Can Geotech J 41(3):523–539

Pan W, Gao Z, Zheng C, Gong Z (2018) Analysis on the influence of cross tunnel construction on the deformation of the existing high-speed railway tunnel. J Geotech Geol Eng 36:4001–4013. https://doi.org/10.1007/s10706-018-0553-4

Plaxis manual (2022) Delft University of Technology & Plaxis bv, The Netherlands

Rieben EH (1966) Geological observation on alluvial deposits in Northern Iran. Geological Organization of Iran, Report, pp 9–39

Sadaghiani MH, Dadizadeh S (2010) Study on the effect of a new construction method for a large span metro underground station in Tabriz-Iran. Tunn Undergr Space Technol 25:63–69

Sadaghiani MH, Gheysar Y (2003) Study on the effect of construction sequence of a large underground on the ground behavior in Mellat Station, Tehran Metro. In: Proceedings, fourth national civil engineering conference, Tehran, Iran, pp 287–294 (In Persian)

Sadaghiani MH, Mirhadi M (2013) Numerical study to investigate the interaction of line 7 of Tehran metro and Tohid tunnel. In: 7th National civil engineering conference

Sadd M (2009) Elasticity, theory, application and numerics, 2nd edn. Elsevier, Academic Publishers, USA

Sagaseta C, Moya J.F, Oteo C (1980) Estimation of ground subsidence over urban tunnels. In: Proceeding of 2nd conference on ground movement and structure. Cardiff, pp 331–344

Sahel Consulting Co. (2015) Geotechnical investigations & foundation report for G7F6 station, Tehran Metro Line 7 Project (In Persian)

Sharifzadeh M, Kolivand F, Ghorbani M, Yasrobi SH (2013) Design of sequential excavation method for large span urban tunnels in soft ground—Niayesh tunnel. Tunn Undergr Space Technol 35:178–188

Tahmasebi MA, Shirinabadi R, Rahimi E, Moosavi E, Bangian Tabrizi AH (2022) Three-dimensional probabilistic analysis of the surface settlement based on spatial variability of soil properties: case study Zarbalizadeh NATM tunnel. J Geotech Geol Eng 40:4895–4910. https://doi.org/10.1007/s10706-022-02189-4

U.S. Department of Transportation Federal Highway Administration (FHWA) (2009) Technical manual for design and construction of road tunnels civil elements.

Valizadeh Kivi A, Sadaghiani MH, Ahmadi MM (2012) Numerical modeling of ground settlement control of large span underground metro station in Tehran Metro using Central Beam Column (CBC) structure. Tunn Undergr Space Technol 28:1–9

Vorster TE, Klar A, Soga K, Mair RJ (2005) Estimating the effects of tunneling on existing pipelines. J Geotech Geoenviron Eng 131(11):1399–1410

Yamaguchi I, Yamazaki I, Kiritani Y (1998) Study of ground-tunnel interactions of four shield tunnels driven in close proximity, in relation to design and construction of parallel shield tunnels. Tunn Undergr Space Technol 13(3):289–304

Zhang Z, Huang M (2014) Geotechnical influence on existing subway tunnels induced by multiline tunneling in Shanghai soft soil. Comput Geotech 56:121–132

Zheng Y, Wu K, Sun J, Chen R, Li Y, Yang S (2021) Study on the influence of close distance construction of urban tunnel on the existing station. J Geotech Geol Eng 39:4765–4780. https://doi.org/10.1007/s10706-021-01790-3

Zhou S, Zhou Z, Liu H, Li L, Li J, Shang C, Ji X (2022) Mechanical response of supporting structure of closely spaced super large span twin tunnels. J Geotech Geol Eng 40:4879–4894. https://doi.org/10.1007/s10706-022-02188-5

Zhou Z, Ding H, Miao L, Gong C (2021) Predictive model for the surface settlement caused by the excavation of twin tunnels. Tunn Undergr Space Technol 114